DIFFUSION IN GOLD-NICKEL ALLOYS

By

JAMES EUGENE REYNOLDS

B. S., University of Alabama

1944

M. S., Missouri School of Mines and Metallurgy

1948

Submitted in Partial Fulfillment of the

Requirements for the Degree of

DOCTOR OF SCIENCE

at the

Massachusetts Institute of Technology

1953

Signature of Author
Department of Metallurgy
November 16, 1953

Signature of Professor
in charge of Research

Signature of Chairman
Department Committee
on Graduate Research

ABSTRACT

DIFFUSION IN GOLD-NICKEL ALLOYS

By

J. E. Reynolds

Submitted for the degree of Doctor of Science

In the Department of Metallurgy, November 16, 1953

Self-diffusion coefficients of Ni^{63} have been determined as a function of concentration and temperature in gold-nickel alloys.

Interdiffusion coefficients have been determined in the gold-nickel system as a function of concentration and temperature, and studies have been made of porosity generation, marker movements, and molar volume changes during diffusion.

Using the above results along with the thermodynamic data from Seigle(10) and the self-diffusivities of Au^{198} determined by Kurtz(11), an attempt was made to test the validity of the Darken equation relating the intrinsic and interdiffusion coefficients with the mobilities and thermodynamics at 850 and 900°C. Good agreement was obtained, and thus it appears that the chemical potential gradient is the valid driving force for diffusion in this system under the conditions studied.

TABLE OF CONTENTS

LIST OF ILLUSTRATIONS

LIST OF TABLES

ACKNOWLEDGMENTS

This investigation was aided considerably by the many people who gave advice and assistance throughout.

Special appreciation is afforded Professors Morris Cohen and B. L. Averbach for numerous consultations.

To Messrs. George Pishenin, Vladimir Czerniszow, Pvt. Edward Keplin, and to my wife who aided in much of the experimental work, I am deeply grateful.

Acknowledgment is due Mr. D. L. Guernsey and his staff who did all of the chemical analyses.

This thesis is part of a research program sponsored by the Wright Air Development Center and appreciation is expressed for their support in this work.

I. INTRODUCTION

In 1933, Matano (1) applied Boltzmann's mathematics to the diffusion data of Grube and Jedele (2) for the nickel-copper system and found that the interdiffusion coefficient ($\tilde{D}$) varied with concentration. The influence of composition was large, and $\tilde{D}$ increased approximately one thousand per cent in the range from pure nickel to pure copper. Furthermore, it was the consensus of opinion at that time, and for some years afterwards, that a single coefficient ($\tilde{D}$) was sufficient to describe the isothermal diffusivity in a metallic system at a given concentration.

In 1933, Jedele (3) presented evidence that $D_1 \neq D_2$ in gold-palladium, gold-nickel, and gold-platinum. Only in recent years, however, have any serious attempts been made to deduce the interrelationships between the various coefficients. The concept of an intrinsic diffusion coefficient has been introduced by Darken (4) who presented a phenomenological treatment based upon the chemical potential gradient as the driving force. Unfortunately this treatment could not be tested experimentally since there was no system for which the intrinsic diffusion coefficients, the interdiffusion coefficients, and the thermodynamic properties were available. Recently, other investigators have measured the thermodynamic properties and the self-diffusion coefficients for gold in the gold-nickel system. The present study describes measurements of the self-diffusion coefficients

---

(1) Refers to references listed on page

of nickel and the interdiffusion coefficients in the same system, and an attempt is made to check the validity of the Darken equations.

Phenomenological Theory

Onsager and Fuoss (5) were apparently the first to propose that the chemical potential gradient and not the concentration gradient, acts as the driving force for diffusion in electrolytes, and Dehlinger (6), with some modifications, attempted to explain experimental diffusivities in the gold-nickel system. More recently, Darken (4) and Le Claire(7) have interpreted new data by assuming the chemical potential gradient as the driving force. On the other hand, Birchenall and Mehl (8), and Guy (9), have been advocates of the activity gradient as the driving force.

Le Claire(7) has clearly summarized the apparent validity of chemical potential as the driving force. Basically, the chemical potentials of the components participating in the diffusion process seem more significant quantities than the concentrations since equilibrium exists in a system only when the chemical potential (μ_i) of each component (i) is the same at every point in each phase throughout the system. It would appear, therefore, that a net diffusion of component from one point to another in a system is possible only when there is a chemical potential gradient ($\frac{\partial \mu_i}{\partial y}$) for component. Since the effect of one component upon the activity of another may be positive or negative, the concentration gradient is not necessarily of the same sign as the chemical potential gradient.

The driving force (z_i) per atom of species i is given by:

$$z_i = -\frac{1}{N_o}\frac{\partial \mu_i}{\partial y} \qquad (1)$$

Where N_o is Avogadro's number, μ_i is the chemical potential per mol of component i, and y is the distance in the diffusion direction. (All of the symbols used in this thesis are defined in Table I) If the mobility (B_i) is defined as the average velocity of species i for a unit driving force, then the average velocity (v_i) of diffusion of the i-th component is given by:

$$v_i = -\frac{B_i}{N_o}\frac{\partial \mu_i}{\partial y} \qquad (2)$$

At constant temperature and pressure

$$\mu_i - \mu_i^o = R\,T\,\ln a_i \qquad (3)$$

where μ_i^o is the chemical potential of i in a standard state, and a_i is the activity of i in a non-ideal solution. R is the gas constant.

The diffusion flux J_i with respect to inert markers in terms of the number of atoms of i passing through an interface of unit area in the y-direction in unit time may be written as

$$J_i = -c_i \frac{B_i}{N_o}\frac{\partial \mu_i}{\partial y} = -D_i \frac{\partial c_i}{\partial y} \qquad (4)$$

where c_i is the number of i atoms per cm^3 of alloy, and D_i is the intrinsic diffusion coefficient of component i. In terms of activities one obtains:

$$J_i = -c_i \frac{B_i}{N_o}\,R\,T\,\frac{\partial \ln a_i}{\partial y} \qquad (5)$$

TABLE I

List of Symbols

$\tilde{D}$	Interdiffusion coefficient
D_i^*	Self-diffusion coefficient
D_i	Intrinsic diffusion coefficient
μ_i	Chemical potential
y	Distance
z_i	Driving force per atom
B_i	Mobility
v	Marker velocity
f_i	Activity coefficient
t	Time of diffusion anneal
V	Molar Volume
c	Concentration
X	Mole fraction
a	Lattice parameter
ξ	Distance parameter
Q	Activation energy
D_o	Frequency factor

Superscript * refers to radioactive isotope.

The activity can be replaced by $f_i X_i$ where f_i is the activity coefficient and X_i is the mole fraction of component i.

Using equations (4) and (5), and $R/N_o = k$, and substituting $N_o X_i/V$ for c (where V = molar volume):

$$D_i \frac{\partial (N_o X_i/V)}{\partial y} = \frac{N_o X_i}{V} B_i kT \frac{\partial \ln f_i X_i}{\partial y},$$

$$D_i \frac{\partial \ln (N_o X_i/V)}{\partial y} = B_i kT \frac{\partial \ln f_i X_i}{\partial y}$$

If V is constant

$$D_i \frac{\partial \ln X_i}{\partial y} = B_i kT \left[\frac{\partial \ln f_i}{\partial y} + \frac{\partial \ln X_i}{\partial y} \right]$$

Dividing by $\frac{\partial \ln X_i}{\partial y}$

$$D_i = B_i kT \left[\frac{\partial \ln f_i}{\partial \ln X_i} + 1 \right] \qquad (6)$$

Equation (6) is identical with that derived by Onsager and Fuoss(5). For a two-component system an equation of form (6) may be written for each component.

$$D_1 = B_1 kT \left[1 + \frac{\partial \ln f_1}{\partial \ln X_1} \right] \qquad (7)$$

$$D_2 = B_2 kT \left[1 + \frac{\partial \ln f_2}{\partial \ln X_2} \right] \qquad (8)$$

Considering the Gibbs-Duhem relation

$$\frac{\partial \ln f_1}{\partial \ln X_1} = \frac{\partial \ln f_2}{\partial \ln X_2} \qquad (9)$$

it readily follows that the intrinsic diffusivities (D_1 and D_2) can differ only insofar as their mobility terms differ because they have identical thermodynamic factors.

It is apparent that the isothermal intrinsic diffusion coefficients are determined by two factors, the first, a mobility term (B_i) characteristic of each component in its environment, and the second, purely thermodynamic term, identical for both components. The second factor in the right-hand members of equations (7) and (8) expresses the deviation of the solution from ideality. For an ideal solution, one obtains the Einstein relation

$$D_i = B_i kT \tag{10}$$

which is valid for self-diffusion or radioactive diffusion, since the concentration of the radioactive tracer is so small it corresponds to diffusion in an ideal solution. Assuming that the properties of the radioactive isotope are identical with those of the stable isotopes except for a slight difference in mass, it follows that the mobility is the same for both and:

$$D_1 = B_1 kT \left(1 + \frac{\partial \ln f_1}{\partial \ln X_1}\right) = B_1^* kT \left(1 + \frac{\partial \ln f_1}{\partial \ln X_1}\right) \tag{11}$$

where B_1^* is the mobility of the radioactive tracer related to D_1^* through equation (10) and determined by diffusing the tracer element into alloys of various concentrations. It is seen, then, that the intrinsic mobilities as a function of concentration may be taken as equal to the mobilities determined from self-diffusion experiments,

but the intrinsic diffusivities differ from the self-diffusion coefficients unless the intrinsic diffusion occurs in an ideal solution.

Considering now a diffusion couple of two different alloys with uniform initial concentrations and assuming no molar volume change, the change in concentration with time at a given y may be represented by Fick's second law:

$$\frac{\partial c_i}{\partial t} = \frac{\partial}{\partial y}\left(\tilde{D}\frac{\partial c_i}{\partial y}\right) \tag{12}$$

where $\tilde{D}$ is the interdiffusion or chemical diffusion coefficient. Generally, two intrinsic diffusion coefficients D_1 and D_2 are required for a complete interpretation of the diffusion process. Darken(4) has derived the relations which follow:

$$\frac{\partial c_i}{\partial t} = \frac{\partial}{\partial y}\left[(X_1 D_2 + X_2 D_1)\frac{\partial c_i}{\partial y}\right] \tag{13}$$

and from equations (7), (8), and (13), it follows that

$$\tilde{D} = (X_1 B_2 + X_2 B_1)\, kT\left[1 + \frac{\partial \ln f_1}{\partial \ln X_1}\right] \tag{14}$$

or using equation (11), equation (15) may be written

$$\tilde{D} = (X_1 D_2^* + X_2 D_1^*)\left[1 + \frac{\partial \ln f_1}{\partial \ln X_1}\right] \tag{15}$$

where D_1^* and D_2^* are the self-diffusion coefficients of components 1 and 2. Thus $\tilde{D}$ may be determined experimentally by two independent methods: (1) the Boltzmann-Matano treatment of interdiffusion data

and (2) use of equation (15) which requires measurements of activity as a function of concentration and determinations of D_1^* and D_2^* as a function of concentration using radioactive tracers.

Interdiffusion coefficients from the two methods may be expected to agree if the relation in equation (15) is valid. Four assumptions were made in the derivation of equation (15), i.e. individual mobilities of the components do exist, the driving force in the diffusion process is the chemical potential gradient, the radioactive mobilities are equal to the intrinsic mobilities, and molar volume is constant.

Assuming unequal mobilities of species 1 and 2, Darken(4) has added a drift to Fick's first law to compensate for the lattice movement relative to the original join and derived the following relation:

$$v = (D_1 - D_2) \frac{\partial X_1}{\partial y} \tag{16}$$

where v is the drift velocity of the lattice measured by marker movement. Velocity is also identified by considering the parabolic relation which is assumed valid in Fick's second law:

$$\frac{y}{\sqrt{t}} = \text{constant} \tag{17}$$

Differentiating with respect to t

$$v = \frac{dy}{dt} = \text{constant } \tfrac{1}{2} t^{-\frac{1}{2}} \tag{18}$$

and substituting equation (17) in equation (18)

$$v = \frac{\Delta y}{2t} \tag{19}$$

where Δy equals the distance traveled by the marker and t is the time of the diffusion anneal. Equation (19) can be utilized to calculate marker velocities (v) and with equation (16) allows a calculation of (D_1-D_2). If D_1, D_2, Δy, and t are known as a function of concentration, then equation (16) will yield marker velocities.

Previous Work on the Gold-Nickel System

Seigle(10) has determined the thermodynamic data given in Table II for gold-nickel alloys at 850°C and 900°C. These functions allow calculations of the thermodynamic factor $(1 + \frac{\partial \ln f_i}{\partial \ln X_i})$ which will be used later in equation (6). The self-diffusivities of gold in the gold-nickel system have been measured, and their temperature dependency determined by Kurtz(11). These data are contained in Tables III and IV. A check can thus be made on the validity of equation (6) (hereafter referred to as the Darken Equation) if measurements are made to determine D^*_{Ni} and $\tilde{D}$ for the gold-nickel system.

Some reports of porosity in gold-nickel diffusion couples have been made. Balluffi(12) noticed that "digging" occurred on the gold side when gold and nickel wires were heated in contact. This phenomenon has been obtained in a large number of other systems when unequal diffusion occurs, and in every case investigated porosity was found to appear in standard type couples of the same materials. This appears, then, as indirect evidence that gold is diffusing more

TABLE II

Thermodynamic Activity

Coefficients of Nickel in Gold-Nickel Alloys (10)

850°C		900°C	
X_{Ni}	f_{Ni}	X_{Ni}	f_{Ni}
.9518	1.020	.9518	1.019
.9485	1.013	.9485	1.012
.8996	1.043	.8996	1.040
.8899	1.068	.8899	1.063
.8524	1.105	.8566	1.073
.8566	1.082	.8524	1.096
.8051	1.173	.8051	1.159
.7961	1.178	.7961	1.162
.7691	1.222	.7694	1.209
.7694	1.224	.7691	1.206
.7336	1.286	.7336	1.265
.6897	1.356	.6897	1.331
.6778	1.381	.6778	1.350
.5880	1.562	.5880	1.510
.5469	1.633	.5473	1.598
.5473	1.622	.5469	1.562
.4825	1.810	.4825	1.720
.48	1.808	.48	1.72
.4596	1.892	.4596	1.788
.3838	2.135	.3838	2.001
.3748	2.23	.38	2.05
.3800	2.175	.3748	2.079
.3111	2.48	.3111	2.271
.2824	2.38	.2569	2.541
.2711	2.50	.2072	2.978
.2569	2.81	.1893	2.789
.2072	3.345	.1511	3.788
.1893	3.38	.1403	3.230
.1511	4.35	.1415	3.776
.1415	4.38	.0894	5.314
.1403	3.84	.0853	5.946
.0853	7.15		
.0894	6.35		

TABLE III

Self-Diffusion Coefficients

Of Gold in the Gold-Nickel System(11)

Atomic % Ni	°C	t x 10^{-5} +	D^*_{Au} ($cm^2 sec^{-1}$)
0	1025	5.15	5.6 x 10^{-9}
	1000	4.77	4.4 "
	950	5.4	2.7 "
	900	4.95	8.9 x 10^{-10}
	850	5.4	2.65 "
	800	4.86	1.8 "
	750	5.89	5.5 x 10^{-11}
20	950	5.94	2.73 x 10^{-9}
	900	5.75	1.65 "
	875	5.94	8.8 x 10^{-10}
	825	5.94	3.88 "
	795	4.95	2.45 "
35 ++	925	6.73	1.06 x 10^{-9}
	875	6.73	4.86 x 10^{-10}
	850	5.82	3.32 "
	850	6.73	3.27 "
50	940	5.94	1.36 x 10^{-9}
	900	5.98	7.42 x 10^{-10}
	850	5.94	3.20 "
	805	5.98	1.52 "
65 ++	925	6.05	4.25 x 10^{-10}
	900	6.05	2.77 "
	850	6.05	1.10 "
80	1000	4.95	5.94 x 10^{-10}
	950	5.36	1.53 "
	910	6.0	8.30 x 10^{-11}
	850	5.4	1.35 "
100	1100	5.75	9.2 x 10^{-10}
	990	6.0	8.95 x 10^{-11}
	900	6.0	1.0 "

\+ Length of diffusion anneal in seconds

++ Determined this investigation

TABLE IV

Frequency Factors and Activation Energies

For Self-Diffusion of Gold in Gold-Nickel System (11)

Atomic % Ni	$D^*_{o,Au}$ ($cm^2 sec^{-1}$)	Q^*_{Au} (cal/mol)
0	0.265	45,300
20	0.05	40,200
35+	0.063	42,700
50	0.091	43,400
65+	0.51	48,800
80	1.1	60,500
100	2.0	65,000

+ Determined this investigation

rapidly than nickel and porosity may be expected in standard type gold-nickel couples. Seith and Kottmann(13) found porosity in a gold-nickel couple but did not study it quantitatively. Their evidence is based upon a single diffusion run for 48 hours at 900°C.

Drift Velocity of the Lattice

Following the work of Smigelskas and Kirkendall (14) da Silva and Mehl(15) established ample evidence that the lattice drift indicated by marker movements is of fundamental importance in diffusion and not uniquely associated with any single system or type of marker material used. Measurements of marker velocities may be used in conjunction with equations (16) through (19) to cross-check intrinsic diffusion coefficients obtained by tracer techniques. It must be kept in mind, however, that the marker velocity is related to D_1 and D_2 only for the concentration associated with the marker.

Vacancy Precipitation

In diffusion studies it is recognized that boundary conditions may be invalidated by the precipitation of vacancies, i.e. porosity generation in the diffusion zone as a result of unequal intrinsic diffusion rates. A standard metallographic technique must be used for a given porosity investigation since the size of the pores observed may be dependent upon the technique. Relatively soft metal tends to smear over, obscuring porosity and it is often advantageous to use an etch-polishing technique to give clean polishing. Electrolytic polishing would eliminate smearing in the softer metals but

the danger of pitting necessitates careful control and interpretation. At the higher diffusion temperatures sintering decreases the size of pores, and the equilibrium number of vacancies increases rapidly with temperature. Since porosity depends upon relative intrinsic diffusion coefficients, length of diffusion period, polishing technique, and diffusion temperature, the measurement of porosity can be quite elusive.

Molar Volume Changes

It has been pointed out by Hartley and Crank(16) and Cohen, Wagner, and Reynolds(17) that if there is a molar volume change in the diffusion zone of a Matano couple, the normal measure of distance (y) becomes ambiguous. Methods of correcting for molar volume changes using modified distance parameters have been published(17).

A treatment of this subject in regard to the present work is given in Appendix A of this report, and data from a nickel-gold diffusion couple have been used in calculations with the modified distance parameter to show the magnitude of the effect of molar volume changes on $\tilde{D}$. It is shown that the errors due to molar volume changes in the gold-nickel system are smaller than the experimental errors and are neglected hereafter.

Statement of Problem

Although diffusion coefficients in the literature are numerous, Darken's approach is as yet untested due to the lack of a complete coherent set of data for a single system. It was the object of the present work to supplement the existing data with additional experiments

and to complete the required data for the gold-nickel system. This system was chosen because it exhibits a single continuous solid solution over a range of approximately 200°C (see Figure 1), and large deviations from Raoult's law have been observed. Large chemical potential gradients exist in this system and thus make it ideal for a test of the chemical potential gradient as the true driving force in diffusion. In addition, the large difference in atomic diameters between gold and nickel(18) would appear to foster a large difference in the intrinsic diffusion coefficients. Suitable isotopes are also available for the study of radioactive diffusivities.

The present work on the gold-nickel system was undertaken, therefore, to determine the interdiffusion coefficients, the intrinsic diffusivities of nickel and the marker velocities, taking into account, if necessary, vacancy precipitation and molar volume changes during diffusion.

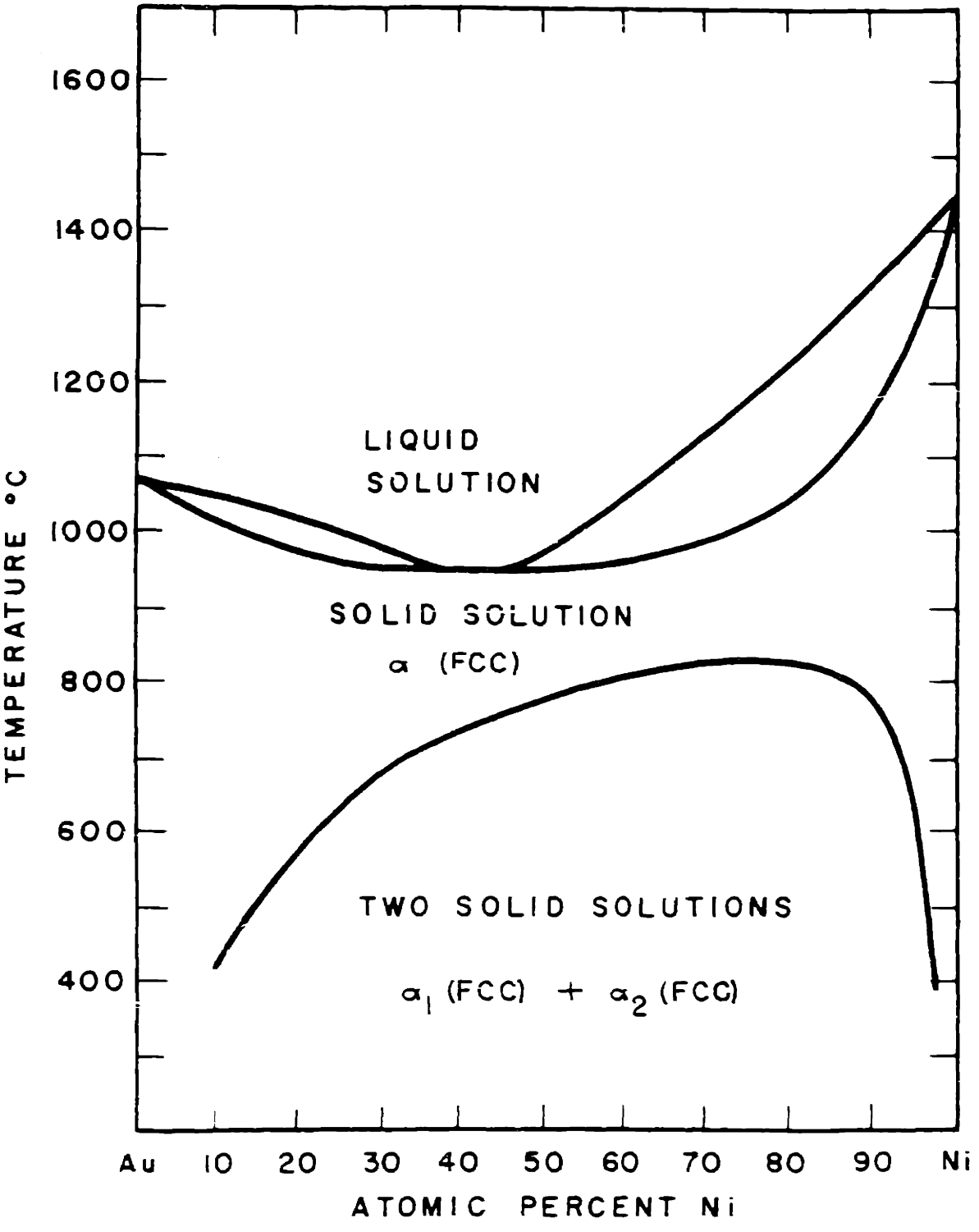

FIGURE 1 - Ni—Au PHASE DIAGRAM

II. EXPERIMENTAL METHODS

Materials Used

Vacuum cast nickel processed by the Vacuum Metals Corporation+ was used for all gold-nickel alloy and pure nickel specimens. The nickel was received in the hot-forged condition, and a photomicrograph of the as-received bar is shown in Figure 2. To minimize contamination from the surface, the bars were turned down from the original 5/8" diameter to $\frac{1}{2}$" and the turnings discarded. A typical chemical analysis is given in Table V. Fine gold from Baker and Co., Inc. was used, and a typical chemical analysis is also given in Table V. Since there is complete solubility of the gold and nickel at the temperatures of interest, the effects of impurities are believed to be unimportant in the present work.

The radioisotope Ni^{63} was used for the measurement of self-diffusion of nickel in the gold-nickel system. It was produced at Oak Ridge by means of the reaction

$$Ni^{62} + n \rightarrow Ni^{63} + \gamma$$

The Ni^{63} was received in the form of nickel chloride in a hydrochloric acid solution with the total activity consisting of more than 95% Ni^{63} activities with less than .01% Ni^{59} activities. The specific activity was about 12mc/gm, and this isotope has a half-life of 85 years. It decays by β emission with particles having a maximum energy of 0.063 Mev.

+ Cambridge, Massachusetts

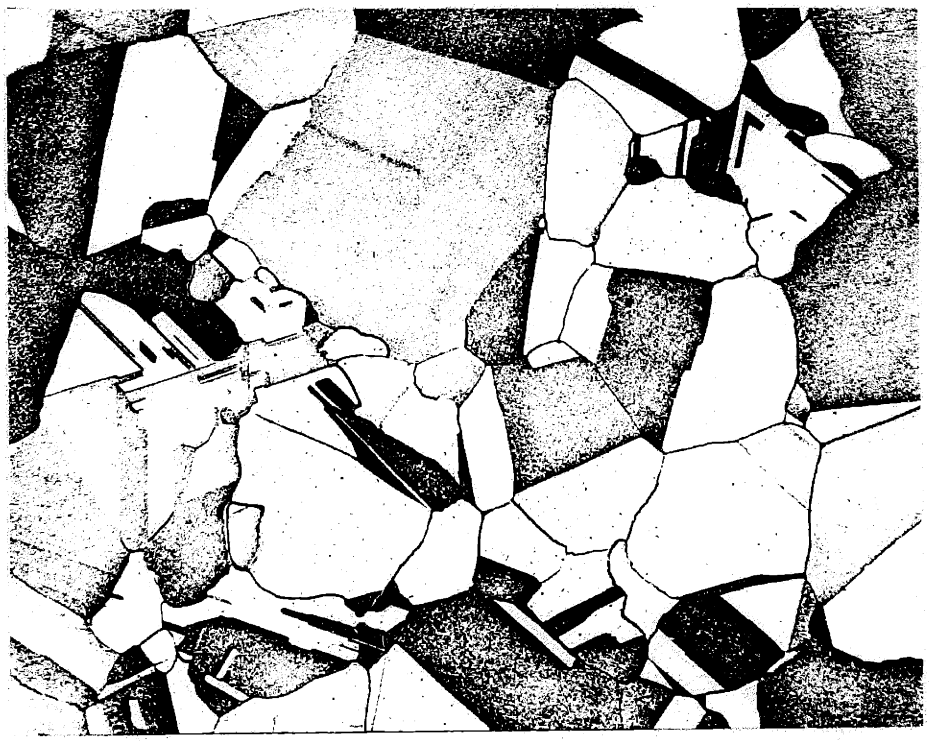

Figure 2 50X

Pure nickel, vacuum cast, hot-forged. Concentrated HNO_3 etch.

TABLE V

Nominal Chemical Analysis of Metals Used

Vacuum Metals Corporation, Vacuum Cast Nickel

Element	Impurity (wt.%)
C	.004
O	.002
N	.000037
Si	.0045
Co	.003
S	.003
Ni	99.986 (by difference)

Baker and Company, Inc., Fine Gold

Element	Impurity (wt.%)
Au	99.96 (by difference)
Ag	.03
Fe	.001
Cu	.002
Pd	.002
Pb	
Si	
Mg	.001
Ca	
Al	
Pt	merest
Rh	spectrographic
Ni	traces of these

Metallic Ni^{63} was extracted from the chloride solution electrolytically, and details of this procedure are given in Appendix B.

Specimen Preparation

Melting Melts were made in a quartz crucible using induction heating, and complete details of the procedure are given in Appendix C. Following solidification, each ingot was given a homogenization treatment. The ingots were sealed under vacuum in vycor and annealed for one week at 925°C to 1000°C (depending on composition). After annealing the ingots were swaged from a diameter of 0.625 to 0.529 inches. This represents a reduction in cross sectional area of 28 percent. After swaging, the ingots were again sealed in evacuated vycor tubes and annealed for one week.

Following homogenization the bars were turned down from 0.529 to 0.500 inches to remove any contaminated surface, and cylindrical specimens for the diffusion couples were made by cutting the bars either with abrasive or high speed steel cut-off wheels. The thickness of the specimens varied from 0.125 to 0.5 inches. The specimens were then gripped in a collet and the ends squared on a lathe. The ends were surface ground so that they were parallel to within $\pm$ 0.0001 inch. The specimens were used without further polishing of the surface.

Mechanical polishing was tried on some specimens, but these invariably yielded bad welds due to the loss of the flat surfaces. It was also noted that gold was "sweated out" by some mechanism in polishing on broadcloth. Either the nickel was removed preferentially

or the gold diffused to the surface preferentially, but a definite gold tint was imparted even to the high nickel alloys after mechanical polishing. All specimens were degreased in benzene before assembly into couples.

Welding All diffusion couples were pressure welded by placing them in a welding unit consisting of a stainless steel (Type 416) cylinder with an inside diameter of 0.625 inch and an outer diameter of 0.782 inch. The inside of the cylinder was threaded and fitted with screw plugs of the same material at both ends. Keyed inserts sandwiching the specimens separated the end plugs from the specimens, thus preventing torsional stresses during the application of pressure. Mica spacers were used wherever welding was not desired, and the plugs were tightened with a 10-inch crescent wrench as tight as one could by hand. The entire unit was placed in a preflushing chamber in argon for 30 minutes before being placed in a tube furnace at 850°C for one hour, also in argon. Cooling was carried out in argon.

Diffusion Anneal Furnaces

Figure 3 shows a schematic drawing of one of the diffusion furnaces. The furnace chamber consisted of a 24-inch alundum tube (Norton Co., Worcester, Mass.) with a 1 3/4-inch bore and a $\frac{1}{4}$-inch wall. Kanthal A wire was wound on the tube -- four turns per inch on the central 9 inches and eight turns per inch for $4\frac{1}{2}$ inches on either side of the central portion, leaving 3 inches on the ends without windings. The core was inclosed in an alundum shield of 3-inch bore and 3/8-inch wall. This shield was then surrounded by

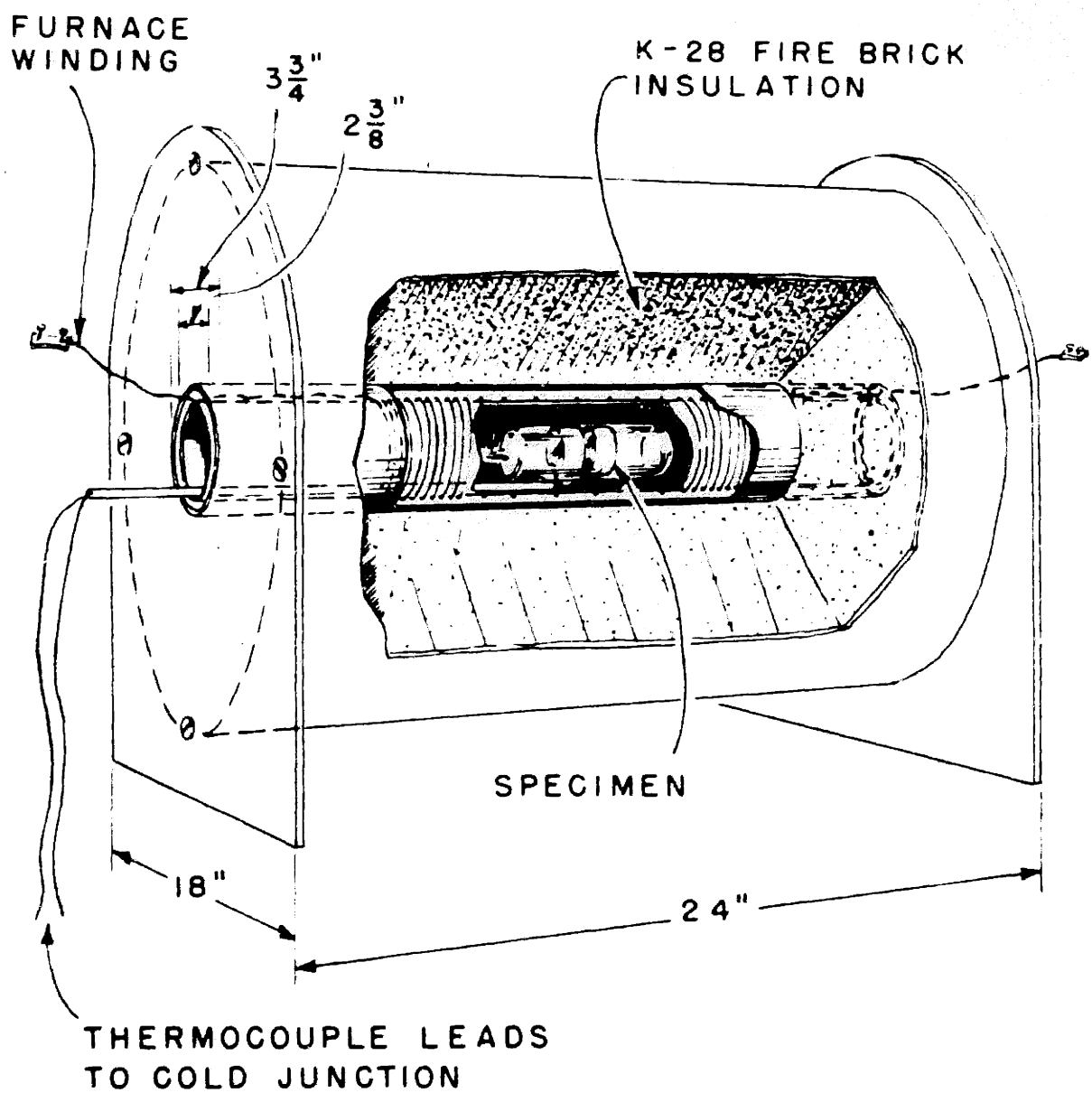

FIGURE 3 - DIFFUSION FURNACE

6 inches of crushed insulating firebrick. The 4-inch central zone in these furnaces had a temperature variation of ±1 degree centigrade. Temperatures were maintained with voltage stabilizers on some furnaces and potentiometric controllers on others, with all of the furnaces being operated in an air conditioned room. Temperatures were measured on a potentiometer to ±0.01 mv (±1°C). Pt-Pt10Rh thermocouples were used.

Self-Diffusion Coefficients of Ni^{63}

Radioisotopes allow one to tag specific groups of atoms which cannot be identified chemically from other groups of atoms and to follow the progress of their migration through the lattice structure. For selected boundary conditions, heat flow mathematics can be utilized to calculate the diffusion coefficients.

Most of these isotope diffusion techniques require the deposition of a thin layer of radioactive material by electroplating or by vaporizing the radioisotope onto the specimen face. Vaporization was used here, and the equipment used is treated in some detail in Appendix D.

Available Techniques Four basically different techniques for measuring diffusivities with the use of tracers may be listed:

1. Sectioning (19,20)
2. Autoradiography (21)
3. Surface-decrease (22,23,24)
4. Surface-increase (25)

Ordinarily the techniques are chosen chiefly on the basis of the magnitude of the diffusion coefficient. Any technique involving the mechanical removal of layers of material parallel to the diffusion interface is necessarily limited to relatively large diffusion coefficients (10^{-10} to 10^{-11} cm^2/sec). The sectioning method, where approximately ten or more slices are taken through the diffusion zone is, therefore, usually limited to coefficients larger than 10^{-11} cm^2/sec. This technique is the most accurate one when coefficients are large, but has the disadvantages of being laborious and requiring reproducible geometry from specimen to specimen in the counting operation.

Autoradiography is also a sectioning method but is much less tedious requiring a single section through the diffusion zone either perpendicular to the original interface or at some other suitable angle if more resolution is needed. The errors in this technique are contingent upon the nature of the isotope used and depend on the type of radiation, the nature of the absorber, and the angle of the section.

Surface counting techniques are important when it is necessary to measure relatively small diffusion coefficients. In the surface-decrease technique the decrease in surface activity is measured resulting from the partial absorption of the radiation from the tracer atoms which have diffused inward. If evaporation of the isotope is significant, then the resulting value of the diffusion

coefficient appears too large. For high vapor pressures, Bakalar(25) has developed a surface-increase technique which involves the sandwiching of the active layer between a cylinder and sheet of inert material and counting the increase in activity through the sheet as the isotope diffuses into the inert materials.

The surface-counting methods are more sensitive than the sectioning method and also less tedious, but the main disadvantage is that a knowledge of absorption coefficients is required.

Autoradiographic Attempt An investigation of the autoradiographic method described by Gatos and Azzam(21) was made using Ni^{63} as a tracer in pure nickel. A layer of approximately 1000 Angstroms of Ni^{63} was deposited on a pure nickel specimen, and with the active face in contact with no-screen X-Ray film for 15 hours, a uniform darkening of the film resulted. This specimen was then welded to a similar specimen (but with no active material) to form the diffusion couple, thereby placing a thin layer of the isotope between two thick pure nickel specimens. After diffusing the couple at 900°C for three days, a section at an angle of approximately 3° with the original join was made through the join and the two oblique faces of the couple were placed on no-screen X-Ray film for as long as 175 hours with no darkening of the film. This was repeated for several different couples at different temperatures, and it was surmised from these tests that the absorption of the weak β particles by nickel was so great that it rendered the autoradiographic method useless for work with the Ni^{63} isotope.

Thus, it appears that the usefulness of the autoradiographic method is limited to isotopes and absorbers with an optimum absorption behavoir. On the one hand, high absorption is desirable so that the radiation will be more indicative of the activity of the sectioned specimen surface, while the other conflicting factor is that the absorptivity must not be so great that registration on the photographic film is prevented.

Surface-Decrease Attempt Some preliminary runs using an end window counter for the surface-decrease technique on single nickel specimens were encouraging in that the diffusion coefficients were of the right order of magnitude, but even with thick layers (10^3 to 10^4 Angstroms) of the isotope the counting rate was only approximately 200 counts per minute, due to the high absorption of the 0.063 Mev β particles in air and in the beryllium window of the geiger tube. A windowless flow counter was also tried, and it was then necessary to decrease the evaporated layer to an approximate maximum thickness of 25 Angstroms in order to get 5000 counts per minute. Higher activity would endanger the accuracy by introducing coincidence errors in the counting. Single specimens of nickel with one active face were again given diffusion anneals in vacuo, for times ranging from 1 to 15 hours. Calculated diffusion coefficients were obviously too high, indicating high vapor pressures, although no discoloration of the vycor tube occurred and no activity could be detected on broken fragments of the vycor tube. Surface diffusion was suspected,

but there was also a lack of activity on the sides of the specimen and the face opposite the active face.

Since the vapor pressure of nickel(26) was apparently significant, a diffusion run was tried with approximately 0.1 atmosphere argon, but the results were the same as before. One specimen was made up in a manner similar to that used by Bakalar(25) where two specimens were placed with active faces about 0.002 inch apart and separated by a rim of pure nickel. The couple was held together by tight wrapping in nickel foil. This apparently did not stop the evaporation or surface diffusion although better results might have ensued had the couple been pressure welded to obtain a better seal.

These unsuccessful attempts may be summarized as follows: (1) the surface-decrease technique does not suffer from evaporation difficulties provided that a layer of the isotope of 10^3 to 10^4 Angstroms thickness is applied, but an end window counter must be used giving an undesirably low counting rate, (2) use of the flow counter puts a maximum limit on the thickness of the isotope layer of approximately 25 Angstroms and with such a small quantity of active material, the evaporation error becomes prohibitive, (3) finally there is the question of the absorption coefficients which would be subject to fairly large errors; this also rules out the surface-increase method which, while eliminating errors due to vapor losses, would still require accurate absorption coefficients.

Sectioning Method Used Data from the surface-decrease attempts with pure nickel specimens gave D^*_{Ni} values of the order of 10^{-12} cm^2/sec, but the temperatures were kept low (about 925°C) to minimize vapor

losses. Since vaporization was no problem in sandwich specimens, higher temperatures could be used to bring the diffusion coefficients into the 10^{-11} cm^2/sec range where the sectioning method could be used. Furthermore, the diffusivities were expected to increase as the gold concentration was increased.

The specimens consisted of a thin layer of Ni^{63} sandwiched between two discs of gold-nickel alloy of the same concentration. The Ni^{63} was evaporated onto the face of one specimen only, and when 200 counts per minute were obtained with the specimen on the first shelf of an end window counter, there was an isotope layer of 10^3 to 10^4 Angstroms (as determined by activity) on the specimen. This proved sufficiently active in all cases for counting the individual slices in the sensitive windowless flow counter after diffusion. Welding was carried out by the method previously described.

After the diffusion anneal in an evacuated tube the specimen was turned down from a 0.500-inch diameter to approximately 0.450 inch, and twenty slices of approximately 0.001 or 0.002 inches were taken from each side of the interface and weighed to $\pm$ 0.1 mgm. From the density, diameter and weight, the thickness of each slice was calculated. This procedure minimized errors in the determination of y.

After sectioning, the slices were prepared for counting by the procedure outlined in Appendix E. This step is a very critical one because the high absorption of the β particles makes it difficult

to obtain constant geometry from specimen to specimen. All counting of the sections was done in a Tracerlab Windowless Flow Counter which is reported to be 100 percent efficient and has a 2π angular coverage. The counting rate data was smoothed by plotting counts per minute above background versus y.

For a thin layer of Ni^{63} of thickness "a" diffusing into a semi-infinite specimen, the solution of Fick's second law according to Carslaw and Yaeger(27) is

$$c/c_0 = \frac{a}{\sqrt{4\pi D^* t}} \exp\left[-y^2/4D^* t\right] \qquad (20)$$

or in an equivalent form:

$$\ln c - \ln c_0 = \ln\left[\frac{a}{\sqrt{4\pi D^* t}}\right] - y^2/4D^* t \qquad (21)$$

For an infinitesimally small layer of the isotope one may differentiate with respect to y^2 and convert to logarithms to the base 10 obtaining

$$\frac{d \log c}{d y^2} = \frac{-1}{9.20\, D^* t} \qquad (22)$$

where c is the concentration of the tracer element and is proportional to the counting rate above background, y is the diffusion distance in cm, t is the time in seconds, and D^* is the self-diffusion coefficient in cm^2/sec. Thus, D^*_{Ni} may be calculated by plotting counting rate on a log scale versus y^2 on a linear scale, and the slope will give D^* when time (t) is known. An example of this calculation is given in Appendix F.

Interdiffusion Coefficients

Assembly of Couples The specimens for determining the interdiffusion coefficients were designed for Matano, marker, and porosity studies and consisted of three disks, the two outer disks being identical and higher in nickel content to conserve gold. Figure 4 shows the manner of assembly of the disks. Two identical diffusion zones were obtained with each set of three specimens. One couple was sectioned for Matano and marker work, and the other was used for porosity studies.

Diffusion Anneal After welding, the specimens were sealed in evacuated vycor tubes and diffused for times varying from 13 to 37 days. Interdiffusion coefficients were determined as a function of concentration for four different temperatures (850°C, 875, 900, and 925) for a wide variety of compositions with additional runs at higher temperatures on some incremental couples near the high nickel side. Following the diffusion anneal all specimens were water quenched to retain the single phase.

Sectioning The specimens were placed in a collet in a precision lathe, and the alignments checked by the use of a surface gage and a magnifying glass while the sample was rotated slowly. At least 0.005 inches of the cylindrical surface was removed to minimize surface effects. Layers 0.003 inches thick and parallel to the original join were removed with a sharp tool and the turnings retained for chemical analysis.

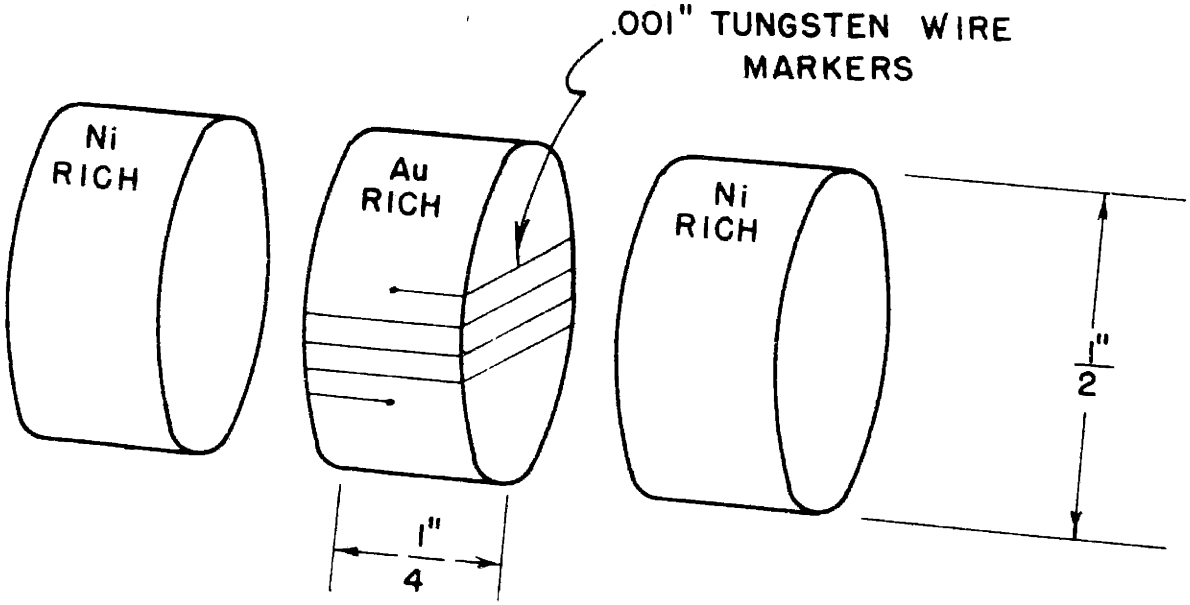

FIGURE 4 - SANDWICH TYPE DIFFUSION COUPLE BEFORE WELDING

Chemical Analyses All chemical analyses were performed in the metallurgy analytical laboratory under the supervision of Mr. D. L. Guernsey. Analyses for both nickel and gold were made — nickel by the dimethylglyoxime gravimetric method, and gold by a standard gravimetric method involving the precipitation of gold with SO_2.

Calculations Details of calculations of interdiffusion coefficients are given in Appendix G in the form of a numerical example. Errors are also treated in that section. A summary of all interdiffusion runs is given in Table VI.

Markers One mil wolfram wire was wound on specimens as shown in Figure 4. A special jig was constructed for winding so that contamination of the degreased faces could be avoided, and the ends of the wire were anchored on the sides with Duco cement. The diffusion curve method for marker movement described by da Silva and Mehl(15) was used in all work here. In machining layers to determine the c-y curve it was noted in which layers the markers appeared; when the markers were uncovered during machining they were easily recognized. The accuracy of locating the markers was, therefore, that of the thickness of the machined layer. Evidence of markers were usually found in several layers (Figure 5), and the center layer in which they were found was taken as their location. Markers seldom remained perfectly parallel to the join as may be seen in Figure 5. Once the markers were located on the c-y curve, the marker shift was measured as the difference between the position of the markers and that of the Matano interface. This is rigorous, however, only

TABLE VI

Summary of Interdiffusion Runs

Run No.	°C	Concentration Limits In Atomic Percent Nickel	Approx. Time In Days
4	850	0 - 100	32
18	"	0 - 20	30
13	"	0 - 35	30
28	"	10 - 50	37
19	"	35 - 65	30
15	"	50 - 80	30
12	"	80 - 100	30
3	875	0 - 100	25
17	"	0 - 20	30
14	"	0 - 35	30
22	"	10 - 50	32
24	"	35 - 65	32
23	"	50 - 80	32
25	"	65 - 90	32
11	"	80 - 100	30
2	900	0 - 100	25
16	"	0 - 20	30
26	"	10 - 50	20
9	"	35 - 65	30
33	"	37 - 95	15
27	"	50 - 80	20
10	"	80 - 100	31
34	"	90 - 100	25
1	925	0 - 100	13
5	"	0 - 20	20
20	"	0 - 35	33
7	"	10 - 50	25
8	"	35 - 65	25
6	"	80 - 100	23
30	950	65 - 100	30
31	"	73 - 100	30
32	975	80 - 100	30

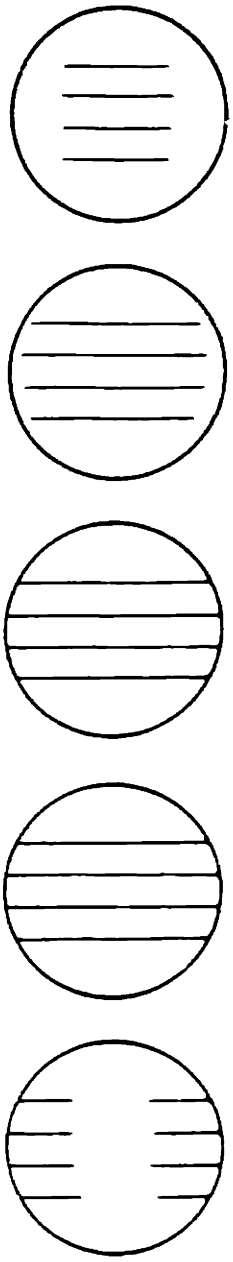

(SUCCESSIVE CUTS .0015")

FIGURE 5 - APPEARANCE OF EXPOSED SURFACES OF SUCCESSIVE CUTS SHOWING ENCOUNTERS WITH MARKERS

if there is correspondence between the Matano interface and the original welding plane i.e. if there is no vacancy precipitation and/or molar volume changes in the zone of diffusion.

Marker velocity (v) was calculated by the use of equation (19) as previously described.

Porosity One couple from each interdiffusion run was sectioned perpendicularly to the diffusion zone and one of the halves mounted in bakelite for metallographic examination. Because of the difficulty in accurately evaluating the nature of porosity, it was necessary to determine the sensitivity of porosity detection for a given metallographic technique. Details of the standard metallographic practice adopted are contained in Appendix H. For pure gold, which presents the greatest difficulty in polishing, it was found that the approximate minimum dimension of a pore that could be detected was 0.5 micron. Etch-polishing techniques were used in studying porosity in the diffusion couples, and it is believed that this gave a better sensitivity than 0.5 micron. Aqua regia was used as the etchant.

III. RESULTS

Self-Diffusion of Ni^{63}

A total of 52 sandwich specimens were prepared for sectioning runs as previously described, and 37 of these yielded usable self-diffusion coefficients the values of which are listed in Table VII. Seven of the runs that were rejected obviously contained bad welds, another was eliminated because of a breakdown in equipment, and the remaining seven runs were lost because of excessive scatter in the counting rates or poor symmetry of the counting rate data about the interface. For most of the usable runs, the scatter was greatest near the peak of the curve of counting rate versus distance.

Activation Energies and Frequency Factors Temperature dependency was determined by the usual method employing the Arrhenius equation:

$$D^*_{Ni} = D^*_{o,Ni} \exp(-Q^*_{Ni}/RT) \qquad (23)$$

Summarized temperature dependency curves are given in Figure 6. For clarification of the data in the high gold region, the curves for 50, 36, 20, 10, and 0 atomic percent nickel have been plotted on a larger scale in Figure 7. Values of the calculated activation energies are tabulated in Table VIII along with the frequency factors ($D^*_{o,Ni}$). With Q^*_{Ni}, D^*_{Ni}, and T for a given concentration, the frequency factor was calculated from the Arrhenius equation. Variation of Q^*_{Ni}

TABLE VII

Radioactive Diffusion Coefficients of Ni^{63} in Au-Ni Alloys

Atomic % Ni	T°C	D^{*}_{Ni} cm²/sec	Approx. time in hrs.
0	937	1.50×10^{-9}	65
	920	1.25 "	49
	904	8.96×10^{-10}	44
	898	8.40 "	72
	880	5.49 "	96
10	940	2.26×10^{-9}	45
	926	1.75 "	66
	880	8.06×10^{-10}	50
20	934	2.13×10^{-9}	47
	930	2.13 "	47
	890	9.65×10^{-10}	45
	880	7.70 "	72
36	920	1.33×10^{-9}	72
	873	5.28×10^{-10}	46
50	925	7.58×10^{-10}	71
	912	5.41 "	50
	903	5.00 "	67
	890	4.06 "	48
	876	3.21 "	50
65	940	3.50×10^{-10}	72
	926	2.85 "	109
	905	2.20 "	89
	882	1.69 "	52
80	999	2.12×10^{-10}	97
	990	2.31 "	48
	962	1.34 "	66
	953	1.09 "	73
	941	1.02 "	105
	940	1.08 "	122
90	1057	1.49×10^{-10}	69
	1025	9.09×10^{-11}	69
	999	7.14 "	97
100	1175	9.83×10^{-11}	62
	1155	6.66 "	65
	1150	5.98 "	83
	1125	4.24 "	97
	1100	2.83 "	188

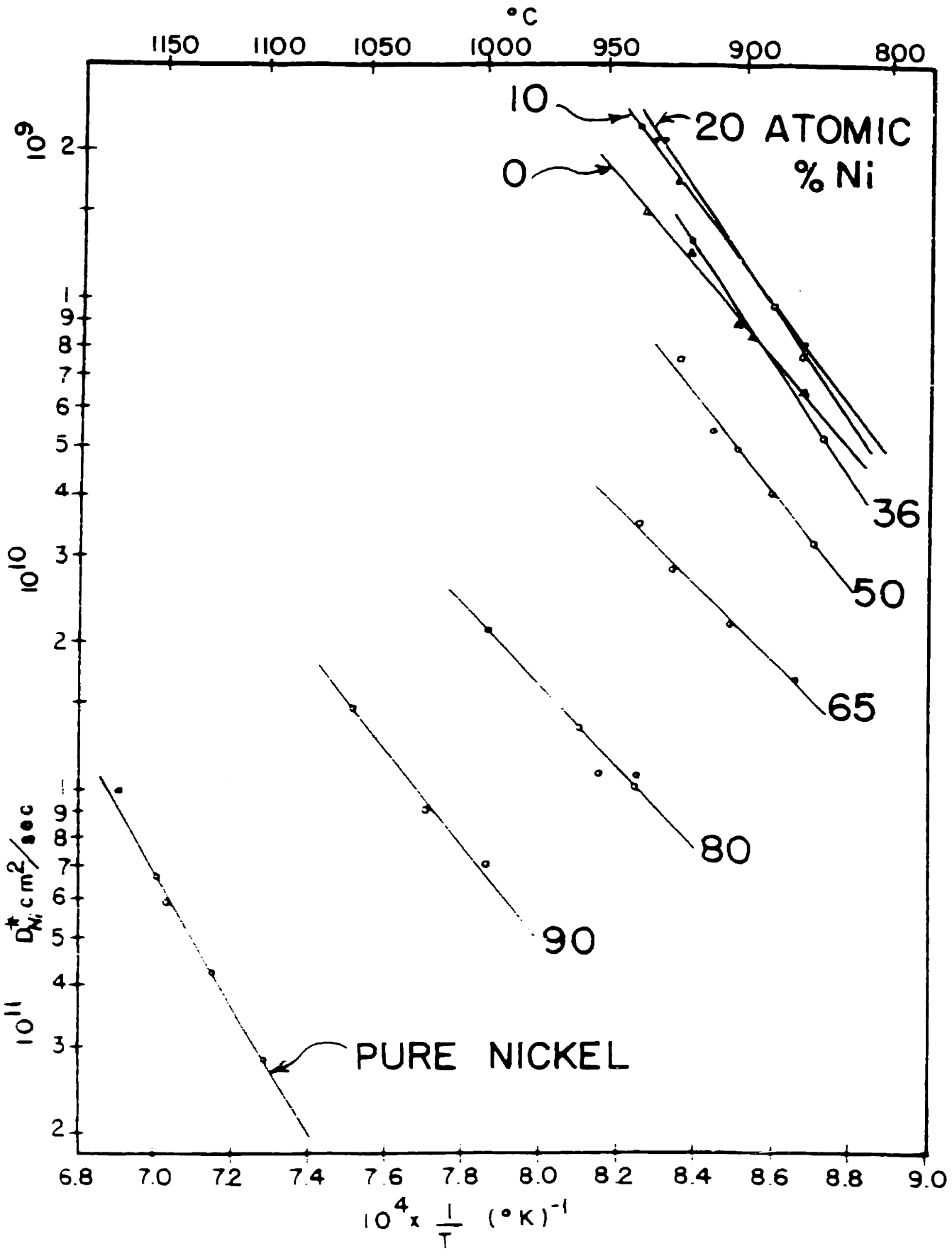

FIGURE 6 - D^*_{Ni} IN GOLD-NICKEL ALLOYS

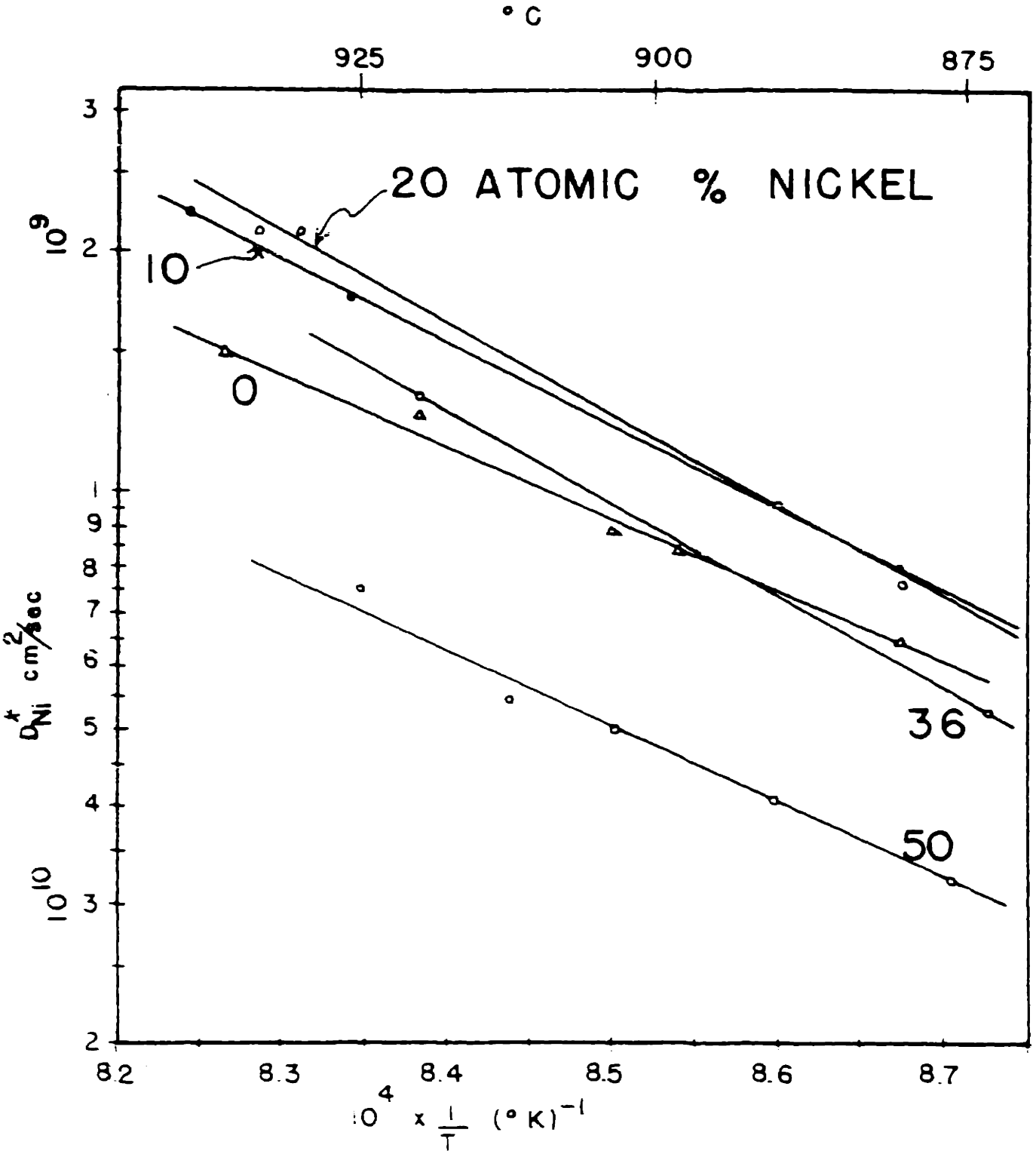

FIGURE 7 - D^*_{Ni} IN GOLD-NICKEL ALLOYS
0-50 ATOMIC % NICKEL

TABLE VIII

Activation Energies and Frequency Factors

For the Self-Diffusion of Ni^{63} in Gold-Nickel Alloys

X_{Ni}	Q^* cal/mol	$D^*_{o,Ni}$ cm^2/sec
0	42,000	6.9×10^{-3}
0.10	48,200	1.09×10^{0}
0.20	53,100	8.94×10^{-1}
0.36	54,400	1.26×10^{1}
0.50	44,300	8.47×10^{-2}
0.65	35,000	7.16×10^{-4}
0.80	39,300	1.2×10^{-3}
0.90	45,300	4.15×10^{-3}
1.00	62,300	2.26×10^{-1}

and $D^{*}_{o,Ni}$ with atomic percent nickel is plotted in Figures 8 and 9 along with similar data for gold.

The diffusivity of Ni in pure gold is a limiting case, but the self-diffusion coefficient representing this limit has been determined by diffusing Ni^{63} into pure gold.

Interdiffusion Coefficients

Successful runs for the calculation of interdiffusion coefficients by the Boltzmann-Matano treatment were summarized previously in Table VI. Calculations were made as described in Appendix G. The resulting $\tilde{D}$ values as a function of concentration are contained in Tables IX through XIII and are plotted in Figures 10 through 14. Where applicable, the limiting values of the self-diffusion coefficients of Ni^{63} in pure gold and Au^{198} in pure nickel were used to smooth the interdiffusion curves at 0 and 100 atomic percent nickel. Concentrations selected for calculations for each run were carefully chosen so as not to approach the limiting concentrations too closely since in these regions the slopes and areas of the gradient curves are most uncertain. The intervals of concentration chosen for calculation were small in order to obtain some smoothing of errors inherent in the calculations. Plots of smoothed data are given in Figure 15.

Temperature Dependence Activation energies and frequency factors were calculated from the interdiffusion coefficients by plotting $\log \tilde{D}$ versus $1/T$ for each concentration of interest and using the Arrhenius equation (Figure 16). Values of $\tilde{Q}$ and $\tilde{D}_o$ are given in Table XIV and plotted in Figures 17 and 18 as a function of concentration.

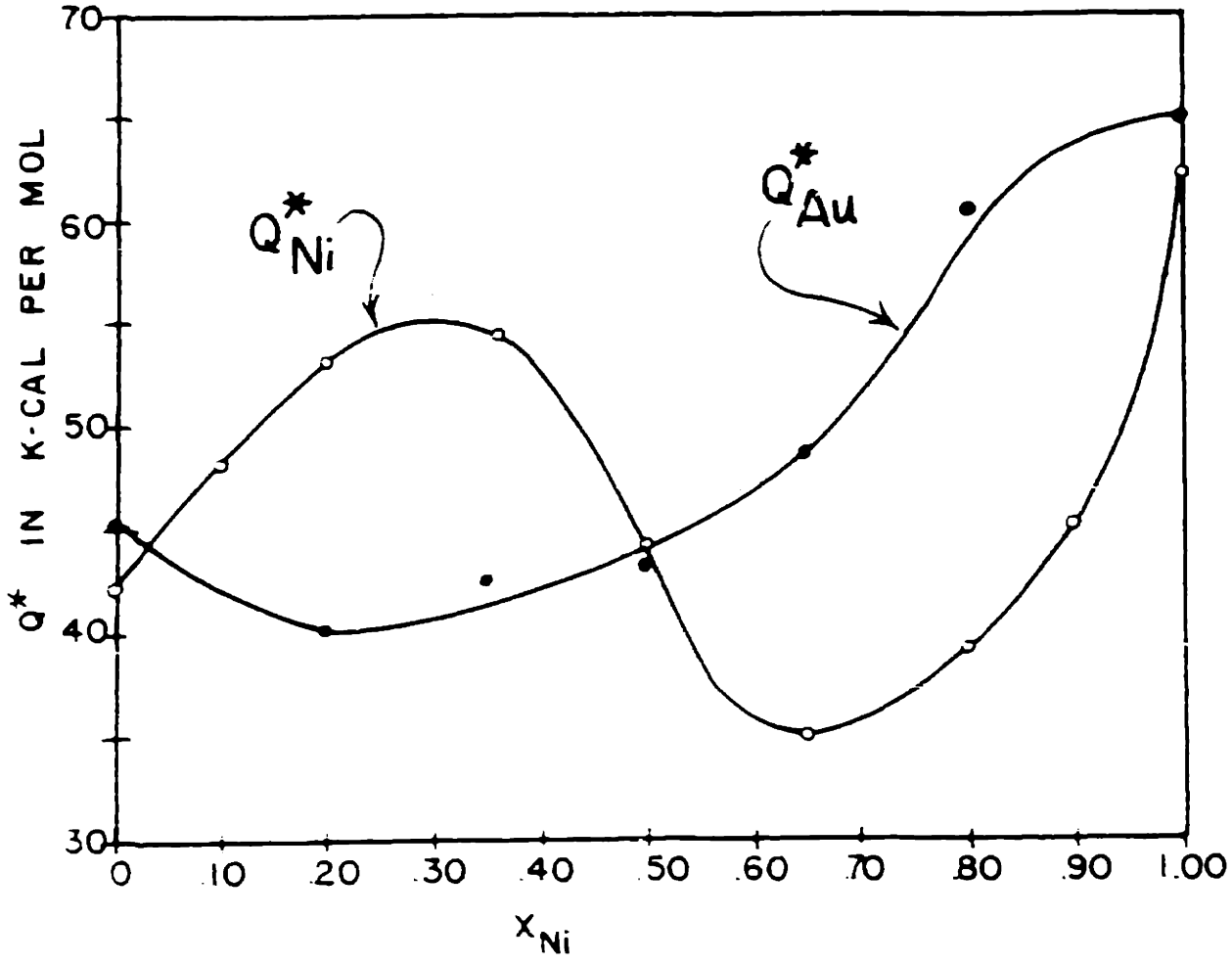

FIGURE 8 - ACTIVATION ENERGIES FOR THE SELF-DIFFUSION OF GOLD AND NICKEL IN THE GOLD-NICKEL SYSTEM

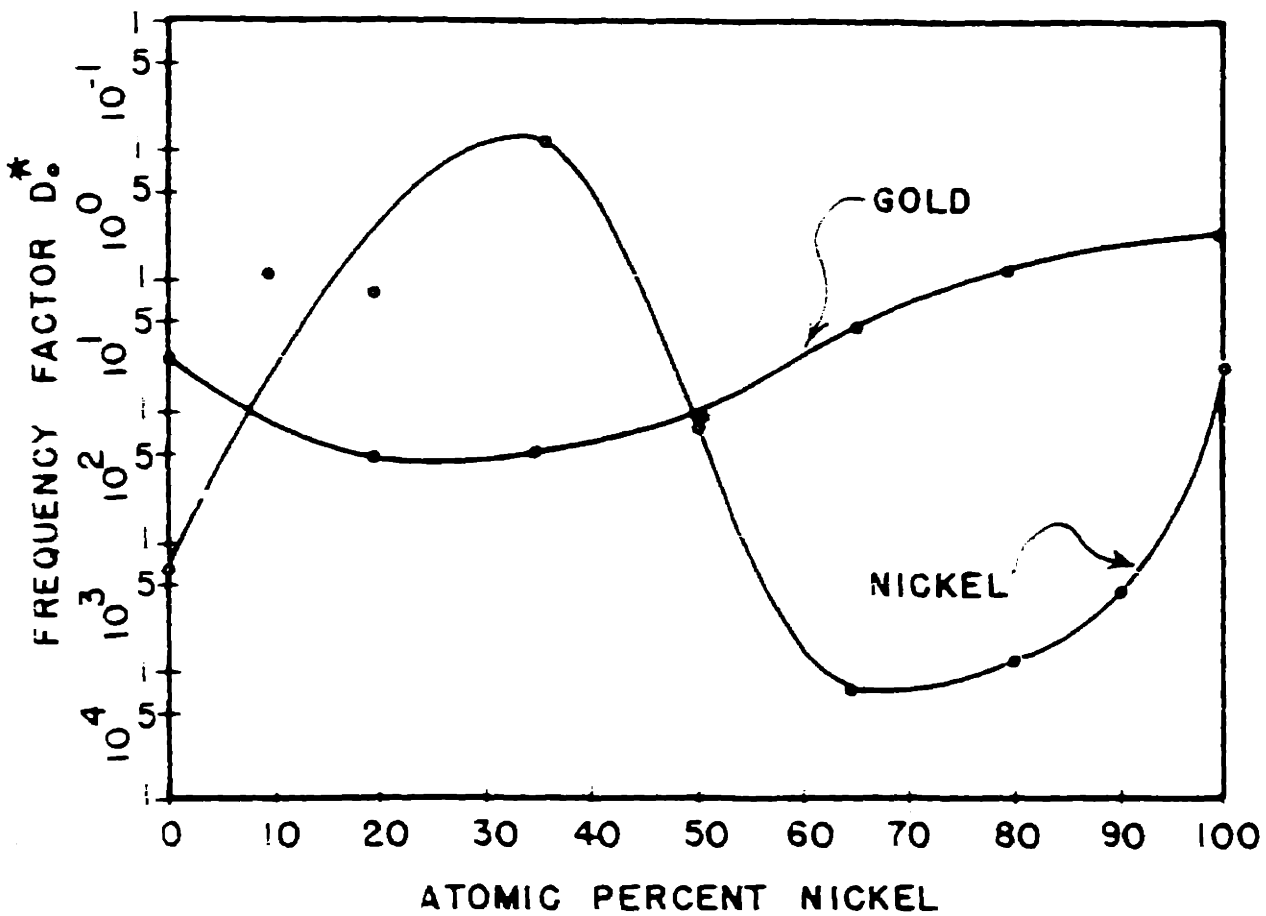

FIGURE 9 - FREQUENCY FACTORS FOR THE SELF-DIFFUSION OF GOLD AND NICKEL IN THE GOLD-NICKEL ALLOYS

TABLE IX

Interdiffusion Coefficients at 850°C

Run No.	Atomic % Ni	$\tilde{D}$ cm²/sec
4	5	4.39×10^{-10}
	10	3.87 "
	15	3.59 "
	20	3.03 "
	25	2.96 "
	30	2.71 "
	35	2.46 "
	40	1.80 "
	45	1.14 "
	50	7.50×10^{-11}
	55	5.05 "
	60	3.78 "
	65	2.89 "
	70	2.41 "
	75	1.23 "
	80	1.46 "
	85	1.76 "
	90	2.38 "
18	3	3.83×10^{-10}
	6	3.67 "
	9	3.37 "
	12	3.32 "
	15	2.77 "
	18	2.90 "
13	3	3.13×10^{-10}
	5	3.58 "
	7	3.35 "
	10	3.14 "
	12	3.33 "
	15	3.66 "
	17	3.56 "
	20	3.11 "
	22	2.95 "
	25	3.10 "
	27	3.24 "
	30	2.94 "
	32	2.40 "
28	20	2.95×10^{-10}
	25	2.45 "
	30	1.76 "
	35	1.44 "
	40	1.29 "
19	40	1.44×10^{-10}
	42	1.27 "
	44	1.07 "
	46	9.06×10^{-11}
	48	8.53 "
	50	7.00 "
	52	6.09 "
	54	4.81 "
	56	3.43 "
	58	2.52 "
	60	1.91 "
15	55	4.30×10^{-11}
	57	4.09 "
	58	3.37 "
	60	2.10 "
	62	1.80 "
	63	1.27 "
	65	1.08 "
	68	1.12 "
	70	1.50 "
	73	1.60 "
	75	1.55 "
	77	1.30 "
12	82	8.65×10^{-12}
	85	7.86 "
	90	5.58 "
	95	5.57 "
	98	4.48 "

TABLE X

Interdiffusion Coefficients at 875°C

Run No.	Atomic % Ni	$\tilde{D}$ cm²/sec
3	5	8.54×10^{-10}
	10	6.96 "
	15	5.76 "
	20	5.24 "
	25	4.61 "
	30	3.80 "
	35	3.16 "
	40	2.29 "
	45	1.83 "
	50	1.18 "
	55	8.28×10^{-11} "
	60	5.96 "
	65	5.73 "
	70	4.96 "
	75	4.59 "
	80	4.10 "
	85	3.67 "
	90	2.98 "
	95	2.17 "
17	3	5.20×10^{-10}
	5	4.53 "
	7.5	5.26 "
	10	4.97 "
	12.5	4.23 "
	15	3.39 "
14	5	4.37×10^{-10}
	10	4.83 "
	15	4.40 "
	20	3.91 "
	25	3.31 "
	30	3.21 "
22	15	4.50×10^{-10}
	20	4.22 "
	25	4.58 "
	30	3.95 "
	35	3.00 "
	40	2.61 "
22	45	2.22×10^{-10}
	48	1.61 "
24	38	2.80×10^{-10}
	42	2.41 "
	46	1.82 "
	50	1.22 "
	54	9.10×10^{-11} "
	58	7.15 "
	60	5.31 "
	62	3.83 "
23	54	6.18×10^{-11}
	56	5.06 "
	58	3.74 "
	60	2.86 "
	62	2.24 "
	64	1.65 "
	66	1.39 "
	68	1.09 "
	70	8.96×10^{-12} "
	72	7.97 "
	74	7.39 "
25	66	1.40×10^{-11}
	67	1.59 "
	69	1.56 "
	71	1.19 "
	73	9.74×10^{-12} "
	75	7.96 "
	77	5.31 "
	79	4.43 "
	81	3.78 "
11	82	5.64×10^{-12}
	84	6.44 "
	88	7.14 "
	92	7.24 "
	96	6.32 "
	98	5.77 "

TABLE XI

Interdiffusion Coefficients at 900°C

Run No.	Atomic % Ni	$\tilde{D}$ cm²/sec
2	5	8.84×10^{-10}
	10	9.85 "
	15	9.55 "
	20	8.82 "
	25	8.00 "
	30	6.56 "
	35	5.47 "
	40	3.82 "
	45	2.98 "
	50	1.93 "
	55	1.43 "
	60	1.01 "
	65	8.91×10^{-11}
	70	6.41 "
	75	5.13 "
	80	4.78 "
	82.5	4.96 "
	85	5.02 "
	87.5	4.25 "
	90	3.51 "
	92.5	3.26 "
	95	3.19 "
16	3	5.01×10^{-10}
	5	4.68 "
	8	4.16 "
	10	4.43 "
	13	4.74 "
	15	4.65 "
26	15	5.83×10^{-10}
	20	7.00 "
	25	5.75 "
	30	5.30 "
	35	4.61 "
	40	3.82 "
9	45	2.30×10^{-10}
	50	2.12 "
	52	1.76 "
	55	1.18 "
	57	6.74×10^{-11}
	60	6.28 "
	62	4.99 "
33+	46	1.70×10^{-10}
	50	1.03 "
	54	7.4×10^{-11}
	58	5.8 "
	62	4.4 "
	66	3.2 "
	70	2.1 "
	74	1.54 "
	78	1.38 "
	80	1.24 "
	82	1.28 "
	84	1.37 "
	86	1.62 "
	88	1.64 "
	90	1.71 "
	92	1.63 "
	94	1.40 "
27	52	9.44×10^{-11}
	54	9.60 "
	56	9.60 "
	58	9.00 "
	60	7.22 "
	62	5.94 "
	64	4.48 "
	66	2.98 "
	68	2.71 "
	70	2.42 "

+ Calculated from experiments by Gatos.

TABLE XI (cont'd)

Interdiffusion Coefficients at 900°C

Run No.		Atomic % Ni	$\tilde{D}$ cm²/sec
27 (cont'd)		72	2.23×10^{-11}
		74	2.21 "
		76	1.63 "
		78	9.03×10^{-12}
10	G*	90	1.75×10^{-11}
		81	1.52 "
		82	1.98 "
		85	2.40 "
		87	2.49 "
		90	1.96 "
		92	1.40 "
		95	9.90×10^{-12}
		98	7.27 "
34	G	95.7	1.10×10^{-11}
		93	1.20 "
		94	1.17 "
		95	1.28 "
		96	1.25 "
		97	1.11 "
35+		3	5.97×10^{-10}
		4.5	6.77 "
		6.0	7.74 "

* G preceding atomic % Ni signifies a Grube calculation instead of the usual Boltzmann-Matano treatment.

+ Calculated from experiments by Gatos.

TABLE XII

Interdiffusion Coefficients at 925°C

Run No.	Atomic % Ni	$\tilde{D}$ cm²/sec
1	5	1.74×10^{-9}
	10	1.72 "
	15	1.65 "
	20	1.47 "
	25	1.47 "
	30	1.27 "
	35	1.16 "
	40	8.77×10^{-10}
	45	6.62 "
	50	3.84 "
	55	2.22 "
	60	1.09 "
	62	5.40×10^{-11}
	65	6.06 "
	67	6.87 "
	70	8.45 "
	72	9.05 "
	75	1.14×10^{-10}
	77	1.17 "
	80	1.38 "
	82	1.21 "
	85	1.08 "
	87	9.36×10^{-11}
	90	9.03 "
	92	8.44 "
5	5	1.49×10^{-9}
	10	1.28 "
	15	9.87×10^{-10}
	20	7.30 "
20	8	2.13×10^{-9}
	10	1.96 "
	12	1.93 "
	14	1.97 "
	16	1.33 "
20	18	1.89×10^{-9}
	20	1.69 "
	22	1.49 "
	24	1.40 "
	26	1.25 "
	28	9.97×10^{-10}
7	15	1.46×10^{-9}
	20	1.26 "
	25	1.13 "
	30	1.04 "
	35	8.48×10^{-10}
	40	6.7 "
	45	3.5 "
8	40	8.90×10^{-10}
	42	6.13 "
	45	5.13 "
	48	4.98 "
	50	4.48 "
	52	3.52 "
	55	2.54 "
	57	2.13 "
	60	1.65 "
	62	1.24 "
6	75	4.54×10^{-11}
	77.5	3.80 "
	80	3.48 "
	82.5	3.97 "
	85	4.31 "
	87.5	4.37 "
	90	4.86 "
	92.5	5.04 "
	95	4.21 "
	96.5	3.48 "

TABLE XIII

Interdiffusion Coefficients at 950°C and 975°C

Run No.	Atomic % Ni	$\tilde{D}$ cm²/sec
30 (950°C)	67	5.37×10^{-11}
	70	5.10 "
	73	4.34 "
	76	3.31 "
	79	3.33 "
	82	3.51 "
	85	3.44 "
	88	3.31 "
	91	2.85 "
	94	2.56 "
	97	2.34 "
31 (950°C)	75	3.96×10^{-11}
	77	4.23 "
	79	3.70 "
	81	3.48 "
	85	3.22 "
	87	2.89 "
	89	2.50 "
	91	2.27 "
	93	2.06 "
	95	1.87 "
	99	1.52 "
32 (975°C)	81	2.47×10^{-11}
	83	2.76 "
	85	2.84 "
	87	2.66 "
	89	3.26 "
	91	3.35 "
	93	2.94 "
	95	2.68 "
	97	2.02 "

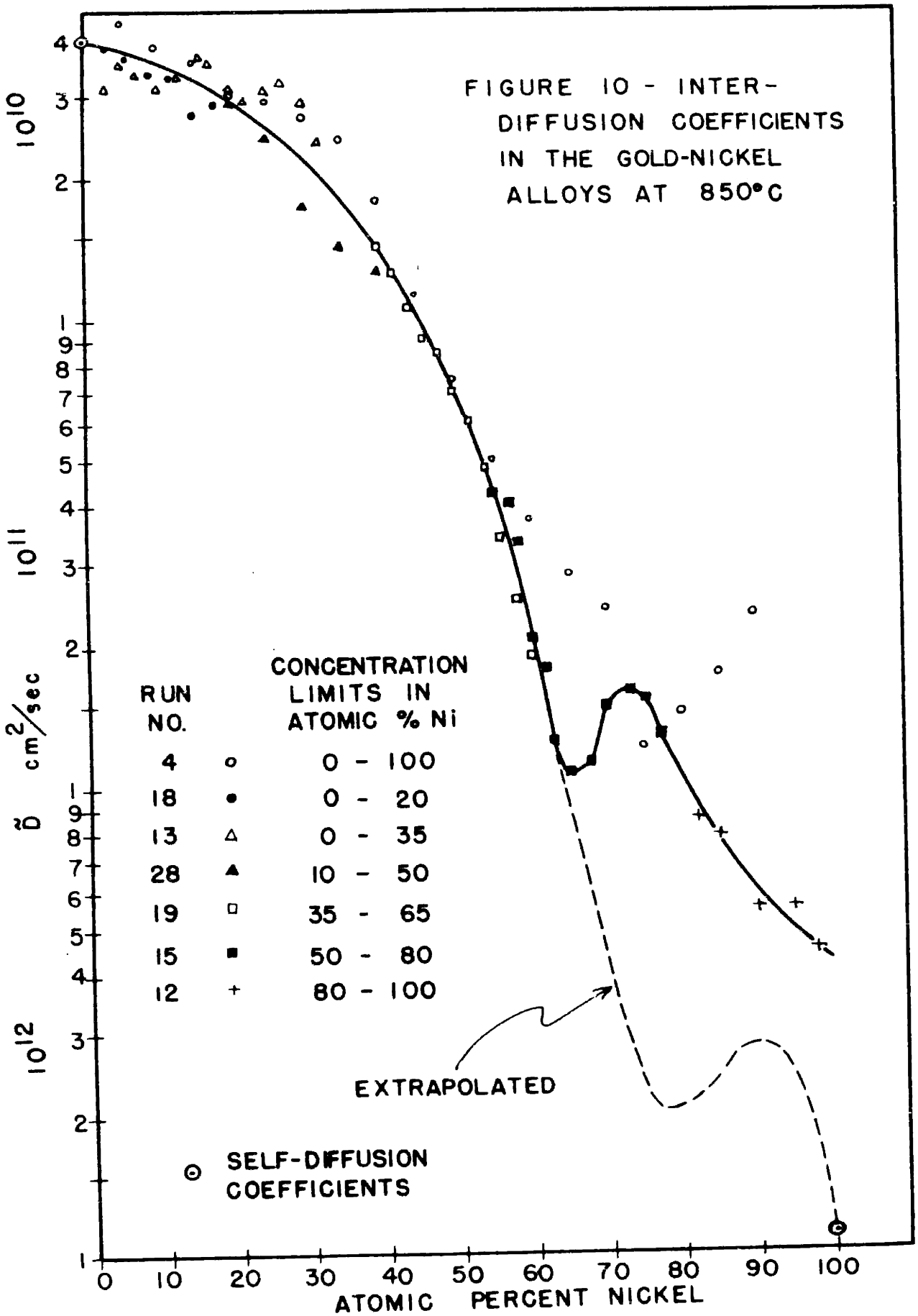
FIGURE 10 - INTER-DIFFUSION COEFFICIENTS IN THE GOLD-NICKEL ALLOYS AT 850°C
D cm²/sec
10¹⁰
10¹¹
10¹²
RUN NO.
CONCENTRATION LIMITS IN ATOMIC % Ni
4 o 0 - 100
18 • 0 - 20
13 Δ 0 - 35
28 ▲ 10 - 50
19 □ 35 - 65
15 ■ 50 - 80
12 + 80 - 100
EXTRAPOLATED
SELF-DIFFUSION COEFFICIENTS
ATOMIC PERCENT NICKEL

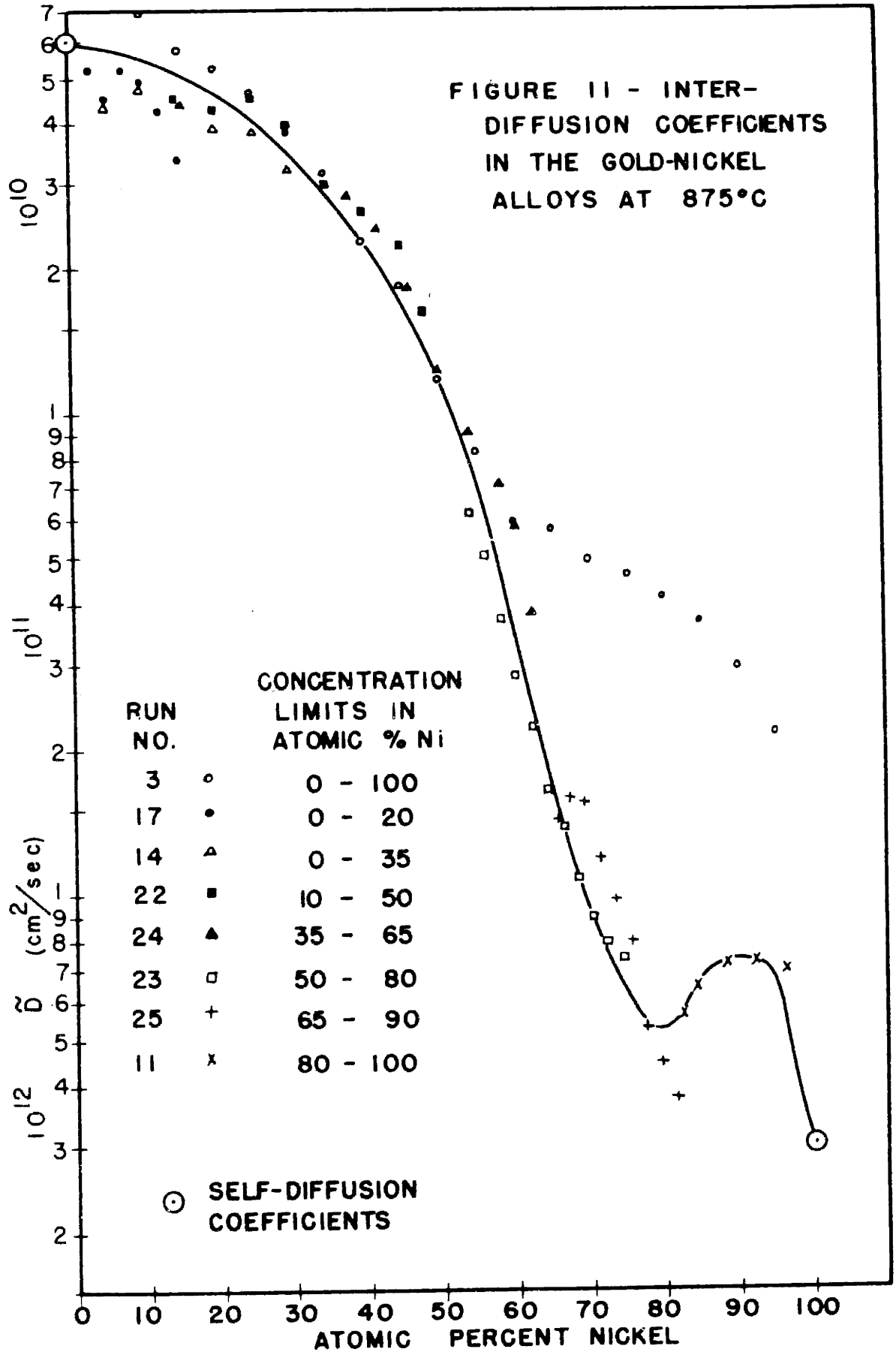
FIGURE 11 - INTER-DIFFUSION COEFFICIENTS IN THE GOLD-NICKEL ALLOYS AT 875°C
CONCENTRATION LIMITS IN ATOMIC % Ni
RUN NO.
3 ○ 0 - 100
17 ● 0 - 20
14 △ 0 - 35
22 ■ 10 - 50
24 ▲ 35 - 65
23 □ 50 - 80
25 + 65 - 90
11 x 80 - 100
SELF-DIFFUSION COEFFICIENTS
D̃ (cm²/sec)
ATOMIC PERCENT NICKEL

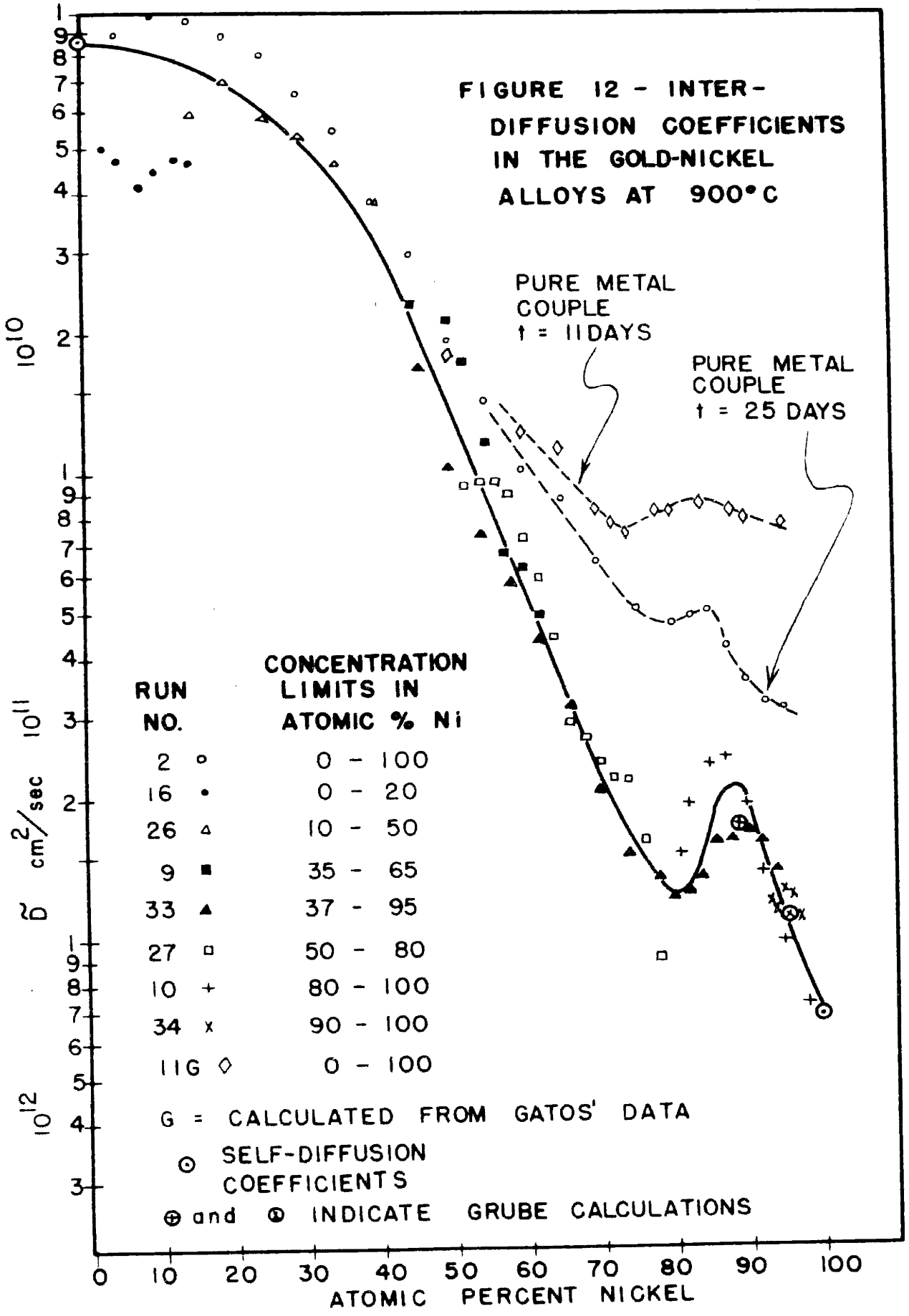
FIGURE 12 - INTER-DIFFUSION COEFFICIENTS IN THE GOLD-NICKEL ALLOYS AT 900°C
PURE METAL COUPLE t = 11 DAYS
PURE METAL COUPLE t = 25 DAYS
CONCENTRATION LIMITS IN ATOMIC % Ni
RUN NO.
2 ○ 0 - 100
16 • 0 - 20
26 △ 10 - 50
9 ■ 35 - 65
33 ▲ 37 - 95
27 □ 50 - 80
10 + 80 - 100
34 x 90 - 100
11G ◇ 0 - 100
G = CALCULATED FROM GATOS' DATA
⊙ SELF-DIFFUSION COEFFICIENTS
⊕ and ⊛ INDICATE GRUBE CALCULATIONS
D cm²/sec
ATOMIC PERCENT NICKEL

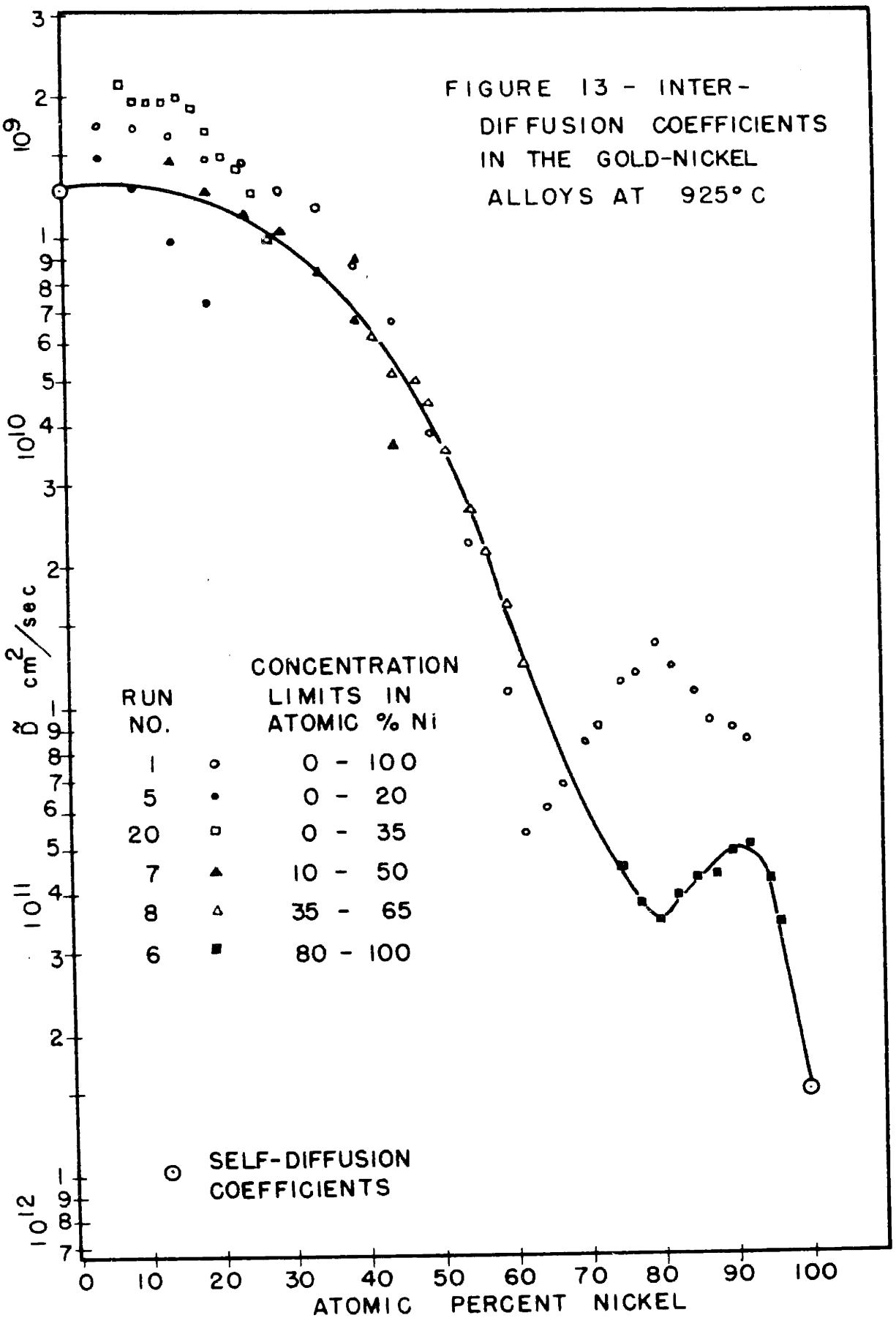
FIGURE 13 - INTER-DIFFUSION COEFFICIENTS IN THE GOLD-NICKEL ALLOYS AT 925° C
D cm²/sec
ATOMIC PERCENT NICKEL
RUN NO.
CONCENTRATION LIMITS IN ATOMIC % Ni
1 ○ 0 - 100
5 • 0 - 20
20 □ 0 - 35
7 ▲ 10 - 50
8 △ 35 - 65
6 ■ 80 - 100
⊙ SELF-DIFFUSION COEFFICIENTS

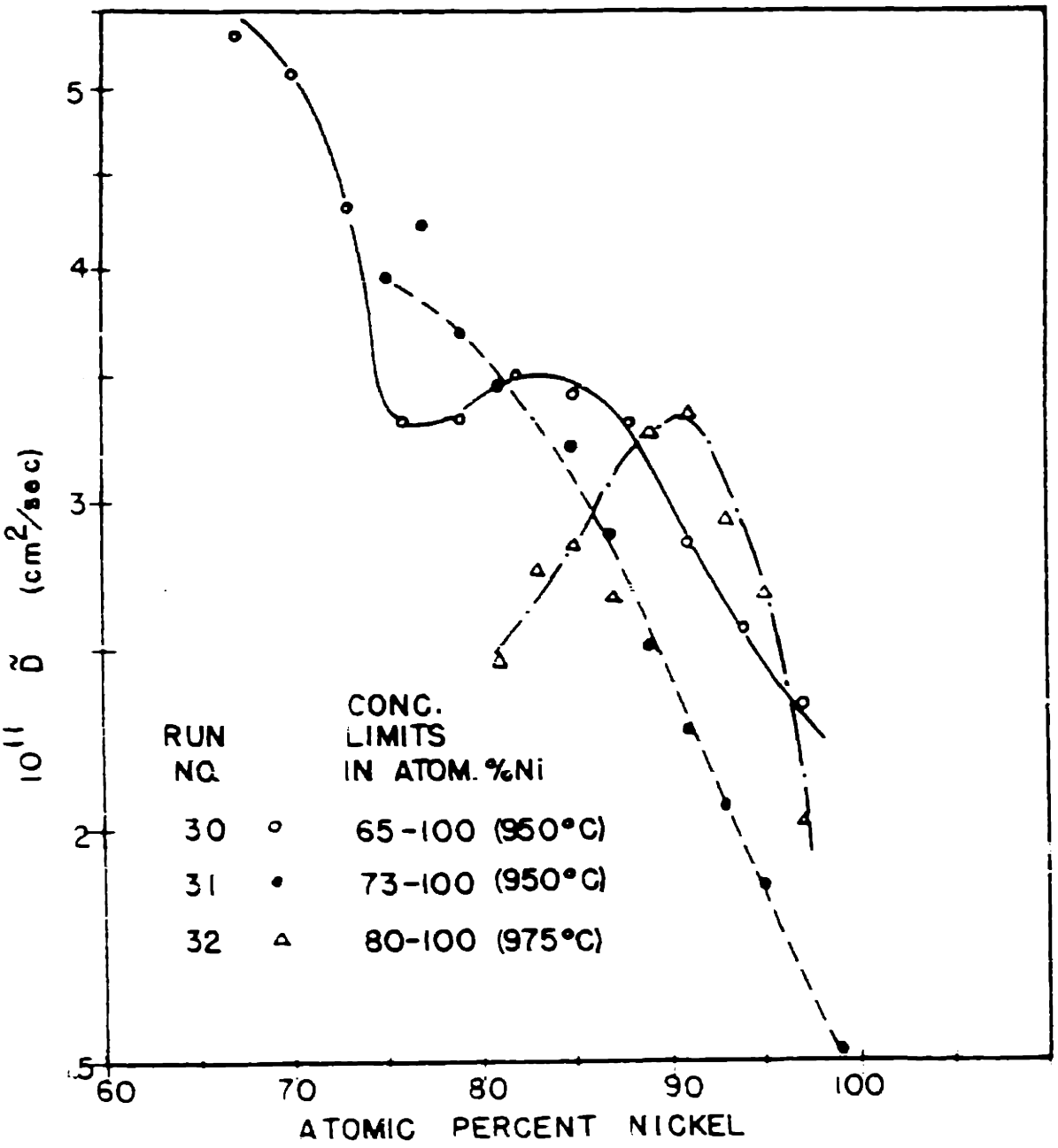

FIGURE 14 - INTERDIFFUSION COEFFICIENTS IN GOLD-NICKEL ALLOYS AT 950°C AND 975°C

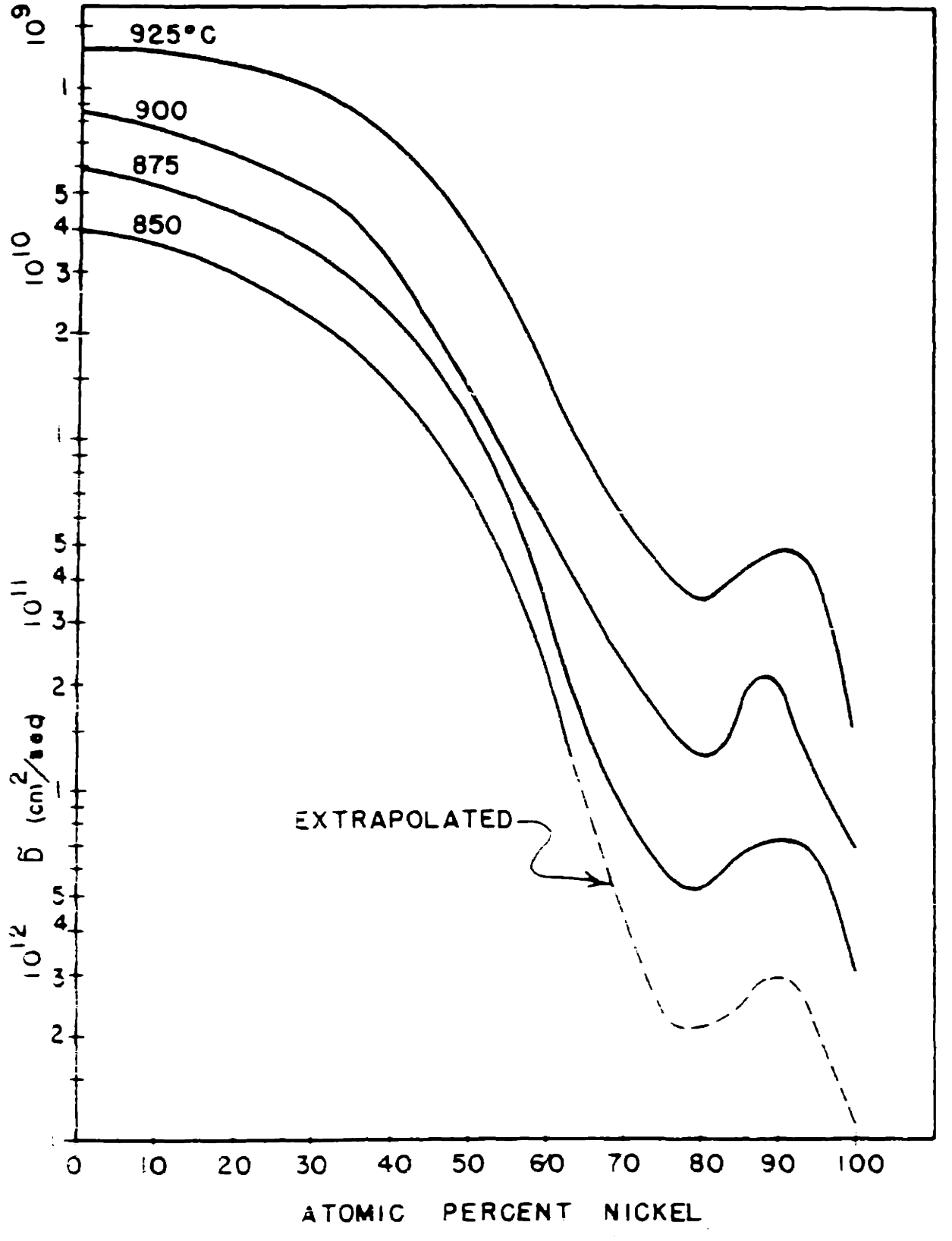

FIGURE 15 – SUMMARY OF INTERDIFFUSION COEFFICIENTS FOR GOLD-NICKEL ALLOYS

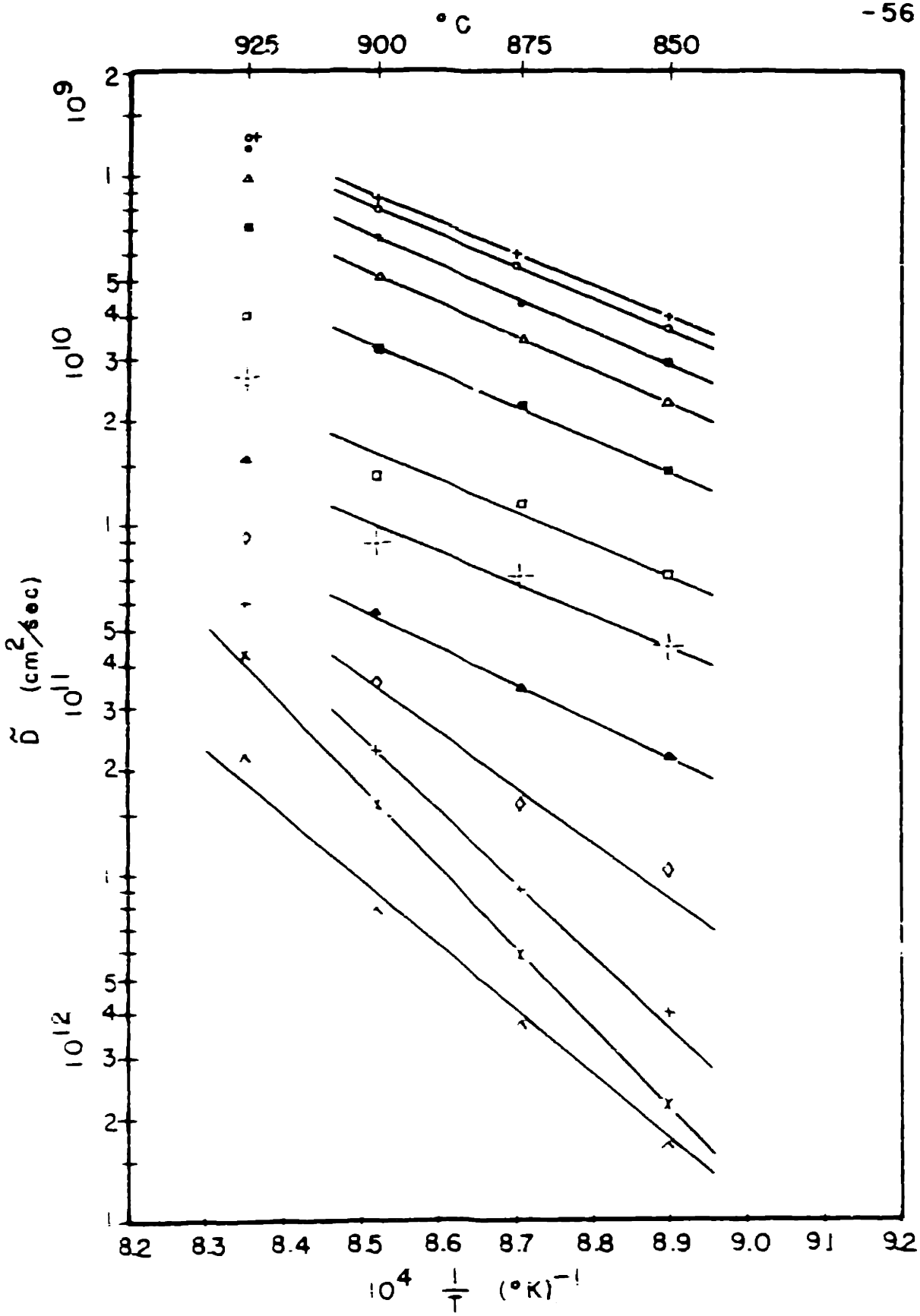

FIGURE 16 – TEMPERATURE DEPENDENCE OF THE INTERDIFFUSION COEFFICIENTS IN GOLD-NICKEL ALLOYS

TABLE XIV

Activation Energies and Frequency Factors for Interdiffusion in Gold-Nickel Alloys

Atomic % Ni	Q Kcal/mol	D_o cm^2/sec
2	41.4	4.3×10^{-2}
10	41.5	3.89×10^{-2}
20	43.7	9.45×10^{-2}
30	43.9	7.80×10^{-2}
40	42.0	2.23×10^{-2}
50	42.4	1.31×10^{-2}
55	41.7	5.87×10^{-3}
60	48.8	6.82×10^{-2}
65	73.0	1.39×10^{3}
70	96.2	1.96×10^{7}
75	105.0	6.15×10^{8}
98	85.2	1.80×10^{4}

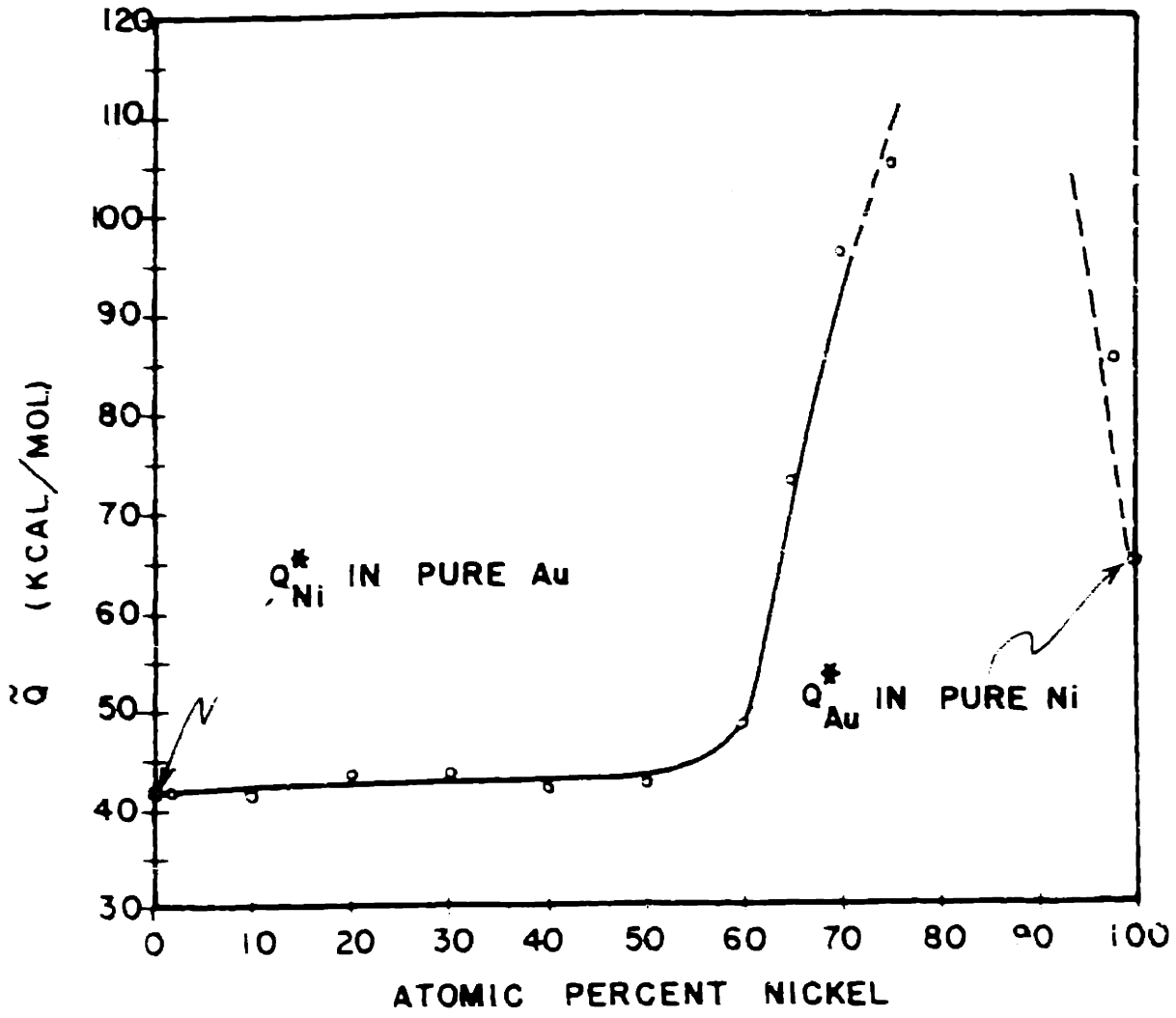

FIGURE 17 - ACTIVATION ENERGIES FOR INTERDIFFUSION IN THE GOLD-NICKEL SYSTEM

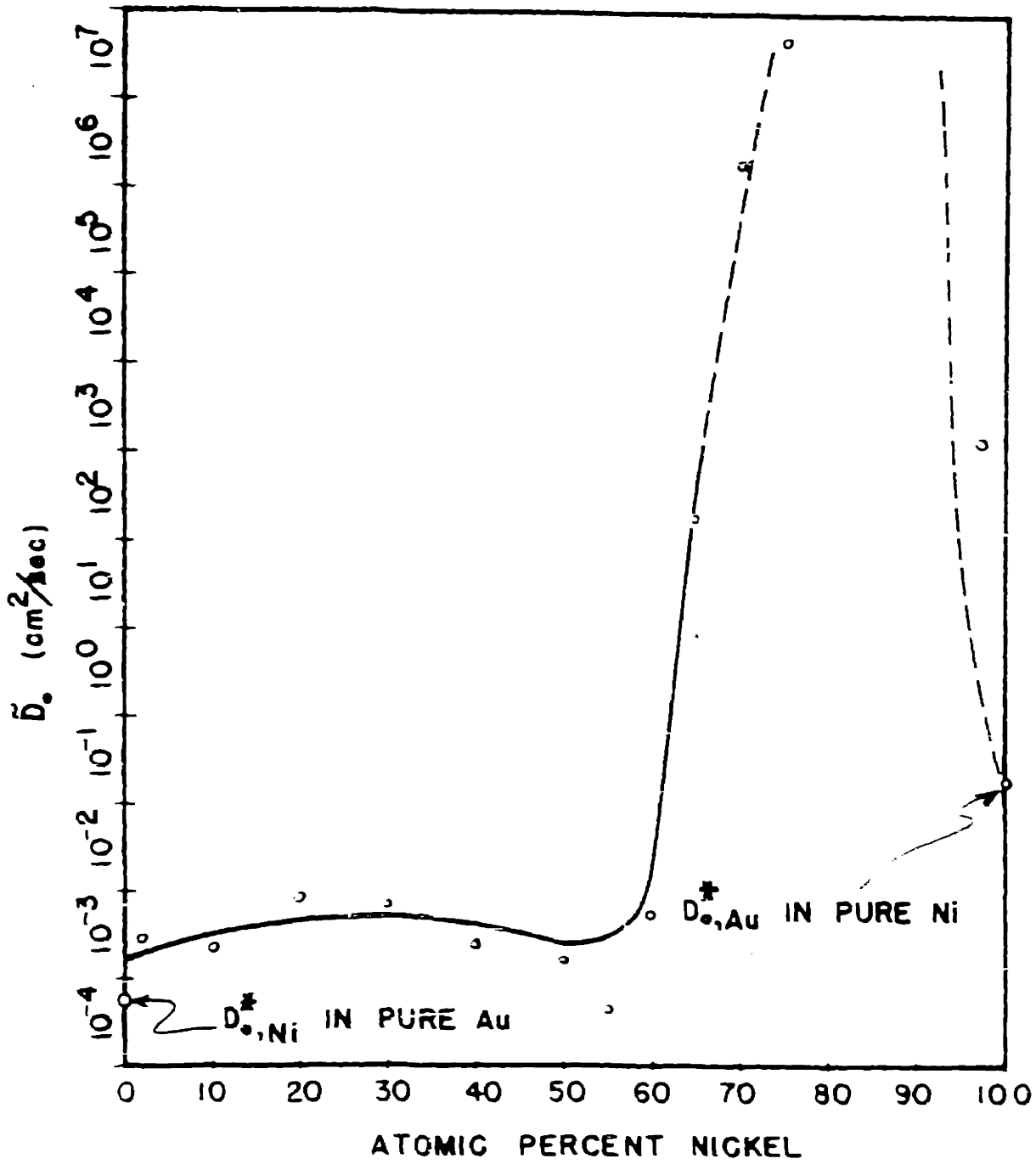

FIGURE 18 - FREQUENCY FACTORS FOR INTERDIFFUSION IN GOLD-NICKEL ALLOYS

Marker Movements Measurement of marker movements was attempted in 17 interdiffusion couples, but the movements were so small that they could not be determined by the diffusion curve method which was used.

Porosity Metallographic examinations of 17 interdiffusion couples were made in the study of porosity. None of the incremental couples showed porosity, but small amounts were found in the pure metal couples diffused at 875, 900, and 925°C. In every instance where porosity was found it occurred on the nickel-rich side of the Matano interface.

IV. DISCUSSION OF RESULTS

Self-Diffusion of Ni^{63}

The diffusion coefficients plotted in Figure 6 appear self consistent, but because of the differences in range of temperature used for the various concentrations it was difficult to obtain D^*_{Ni} values at high and low temperatures completely across the diagram. Extrapolated data have larger errors due to the magnification of the errors in slope. Values of D^*_{Ni} have been taken from the smoothed data, extrapolated where necessary, and plotted in Figure 19 as a function of concentration for several different temperatures. Smoothed data for D^*_{Au} is plotted in Figure 20. It has been shown previously (equations 10 and 11) that

$$D^*_i = B^*_i kT = B_i kT$$

Thus, the intrinsic mobilities are directly proportional to the self-diffusion coefficients differing from them only by the constant factor kT. It then follows that the plots of D^*_{Au} and D^*_{Ni} in Figures 19 and 20 also represent the variation of the mobilities with concentration.

Referring to Figure 8, the variation in Q^*_{Ni} with concentration is surprising since increasing the nickel content from pure gold increases the activation energy to a maximum at a point near the minimum in the liquidus temperature. Contrary to these facts, the

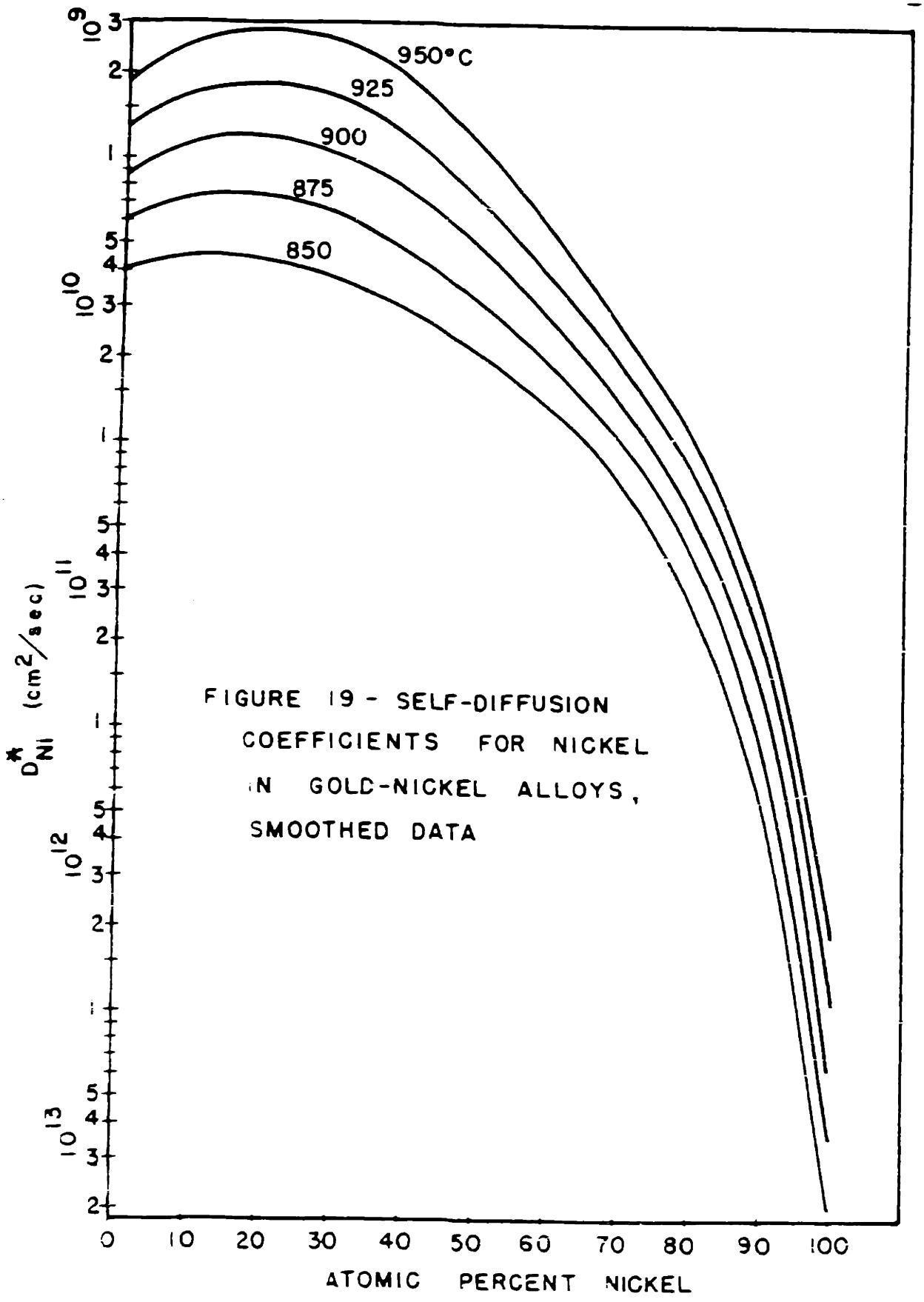

FIGURE 19 - SELF-DIFFUSION COEFFICIENTS FOR NICKEL IN GOLD-NICKEL ALLOYS, SMOOTHED DATA

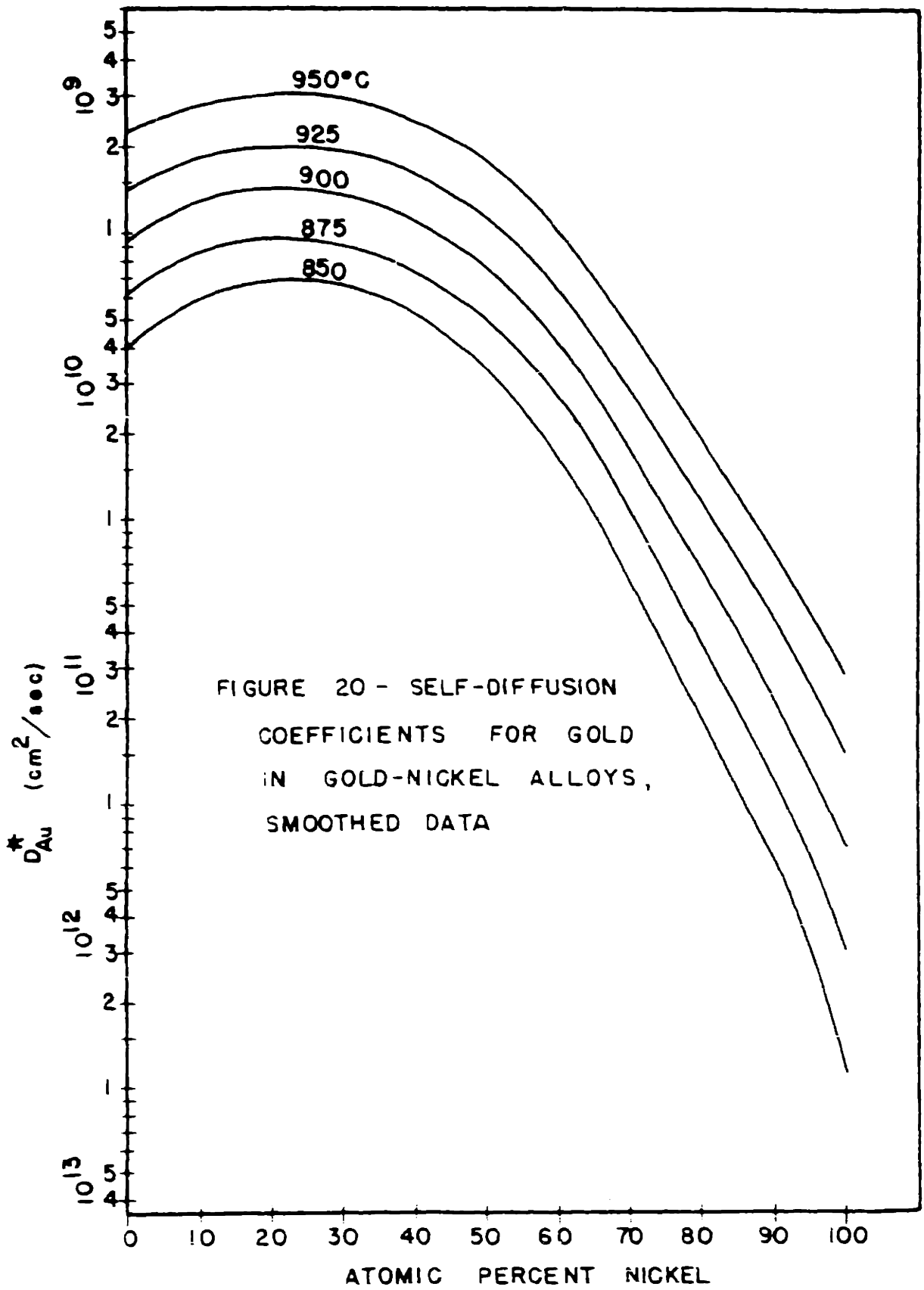

FIGURE 20 - SELF-DIFFUSION COEFFICIENTS FOR GOLD IN GOLD-NICKEL ALLOYS, SMOOTHED DATA

diffusion rate appears to be a maximum near the minimum in the liquidus. Further addition of nickel causes Q^*_{Ni} to drop to a minimum near the high nickel region. da Silva and Mehl (15) have reported a similar variation of the activation energy for inter-diffusion in the copper-nickel system with a maximum also occurring nearer the low melting point constituent. It is interesting to note in Figure 8 that Q^*_{Au} (Kurtz) does not show a maximum but has a pronounced minimum under the minimum in the liquidus.

As may be seen from Figure 19, D^*_{Ni} does not reflect the behavior of Q^*_{Ni} under the minimum in the liquidus, but as is expected from the diagram D^*_{Ni} reaches a maximum in that vicinity, more pronounced as the liquidus is approached. The frequency factor $D^*_{o,Ni}$ changes through four orders of magnitude in going from pure gold to pure nickel and reflects the shape of the Q^*_{Ni} curve exponentially.

Interdiffusion Coefficients

Coefficients were plotted on a separate graph for each temperature because of the scatter of data, and an attempt was made to draw the best smooth curve through each set of data ignoring in every case the data from the 0-100 atomic per cent nickel wide range couple. The wide range data on each graph in Figures 10, 11, 12, and 13 are given by the open circles and do not coincide with the data from the incremental couples. Note especially Figure 12 which has two wide range couples. In most cases the wide range data lies above the incremental data. These discrepancies cannot be ascribed to molar volume changes in the

diffusion zone since this effect would cause somewhat higher coefficients on the side nearest the metal with the smaller lattice parameter and opposite effects nearer the other pure metal, nor can they be due to porosity generation according to the present investigation. Furthermore, it is unlikely that the discrepancies between pure metal and incremental couples are due entirely to molar volume changes or porosity in the diffusion zone since these factors would cause an increase in the errors with time, while the converse is true, the data from pure metal couples tending to approach those of the incremental couples with longer times. Perhaps the cause lies in local strains due to large initial molar volume changes, recrystallization, a lack of steady state conditions in the shorter diffusion anneals, or short circuiting paths accompanying vacancy precipitation.

When the data for 850, 875, 900, and 925°C are plotted on the same graph (Figure 15) and the temperature dependency investigated, it is found that the curves for 850, 875, and 900°C give correlations up to approximately 65 atomic percent nickel and curves for 875 and 900°C up to 75 atomic percent nickel. Calculations for activation energies in the intervening region between 75 and 98 atomic percent nickel were found impossible with the available data.

The "sinusoidal" variation of $\tilde{D}$ is found near high nickel in every instance and for the three higher temperatures the minimum occurred at 80 atomic percent nickel. This is also true for the incomplete data (Figure 14) at 975°C. The portion of the curve for 850°C between 65 and 100 atomic percent nickel (Figure 10), however,

appears incorrect since the curve must lie below that for higher temperatures unless there is a change of diffusion mechanism. It is more likely that the curve is in error, and an extrapolated curve has been added.

Interdiffusion data for 925°C while being self-consistent does not fit into the temperature dependency curves plotted in Figure 16. The $\tilde{D}$ values appear too high. No explanation is offered here for this misfit since the curve has been determined by five independent runs using incremental couples, and it is improbable that these runs would have identical errors. Furthermore, if this curve is indicative of a higher temperature mechanism in operation, then activation energies for this mechanism are greater than 100,000 cal/mol for high gold alloys. It might be added that correspondence of the 925°C data is poorest near high gold and appears to become valid when the nickel has been increased to 75 atomic percent.

Activation Energies Figure 17 contains the variation of the activation energy for interdiffusion with the concentration. The most outstanding feature is the rapid increase in $\tilde{Q}$ as the nickel content is increased toward the composition (80 atomic percent nickel) where the minimum is found in the $\tilde{D}$ curves. Using equation (15) one may write for interdiffusion in the gold-nickel system

$$\tilde{D} = (X_{Ni} D_{Au} + X_{Au} D_{Ni}) \qquad (25)$$

At pure nickel

$$\tilde{D} = X_{Ni} D_{Au} = D_{Au} = D^*_{Au} \qquad (26)$$

and at pure gold

$$\tilde{D} = X_{Au} D_{Ni} = D^*_{Ni} \qquad (27)$$

It follows from equations (26) and (27) and the Arrhenius equation that $\tilde{Q}$ in pure nickel is equal to the activation energy for the self-diffusion of gold in nickel, and $\tilde{Q}$ in pure gold is equal to the activation energy for the self-diffusion of nickel in pure gold. These limiting values of activation energy have been placed in Figure 17, and the curve extrapolated to these values.

Thermodynamic Correlation The only thermodynamic data available above the solubility gap in the gold-nickel system is for 850 and 900°C. Considering the activity coefficients (from Seigle) given in Table II, the self-diffusivities of gold (from Kurtz) in Table III, and the self-diffusion coefficients of nickel in Table VII, a test of the validity of the Darken equation (equation 15) may now be attempted. It is recalled that this equation is

$$\tilde{D}_{calc} = (X_{Ni} D^*_{Au} + X_{Au} D^*_{Ni}) \left[1 + \frac{\partial \ln f_{Ni}}{\partial \ln X_{Ni}}\right] \qquad (15)$$

where X is mol fraction, D^* is the self-diffusion coefficient, and the bracketed term is the thermodynamic factor (Table XV) which is plotted in Figure 21. Evaluating Darken's equation for various compositions gives values of "calculated" interdiffusion coefficients ($\tilde{D}_{calc}$), and if equation (15) is valid, we would expect correspondence between these and the observed values of the interdiffusion coefficients ($\tilde{D}_{obs}$) which have been given in Figures 10 and 12. Figures 22 and 23

TABLE XV

Thermodynamic Factor $(1 + \frac{\partial \ln f_{Ni}}{\partial \ln X_{Ni}})^{+}$

X_{Ni}	$(1 + \frac{\partial \ln f_{Ni}}{\partial \ln X_{Ni}})^{++}$	X_{Ni}	$(1 + \frac{\partial \ln f_{Ni}}{\partial \ln X_{Ni}})$
.05	.531	.60	.2
.10	.47	.62	.18
.15	.435	.65	.142
.20	.420	.68	.103
.25	.407	.70	.08
.30	.40	.72	.052
.35	.40	.75	.032
.40	.397	.78	.018
.45	.378	.80	.019
.50	.335	.82	.027
.55	.275	.85	.055
.60	.220	.88	.140
.65	.160	.90	.225
.70	.100	.95	.505
.73	.070	1.00	1.00
.75	.053		
.77	.045		
.80	.042		
.82	.060		
.85	.120		
.88	.225		
.90	.335		
.92	.455		
.95	.645		
1.00	1.00		

+ calculated from the data of Seigle.
++ calculated by Kurtz.

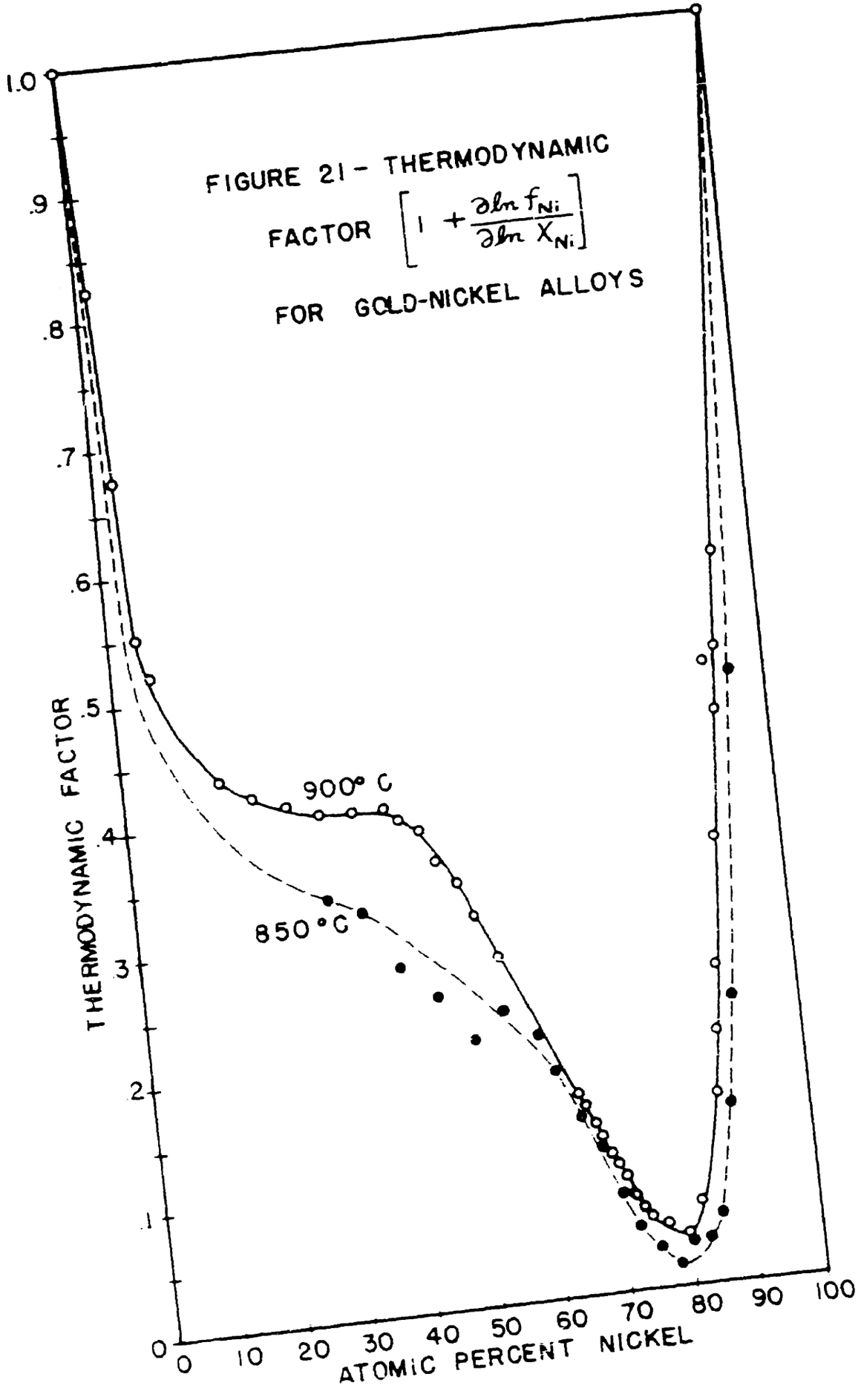

FIGURE 21 - THERMODYNAMIC FACTOR $\left[1 + \frac{\partial \ln f_{Ni}}{\partial \ln X_{Ni}}\right]$ FOR GOLD-NICKEL ALLOYS

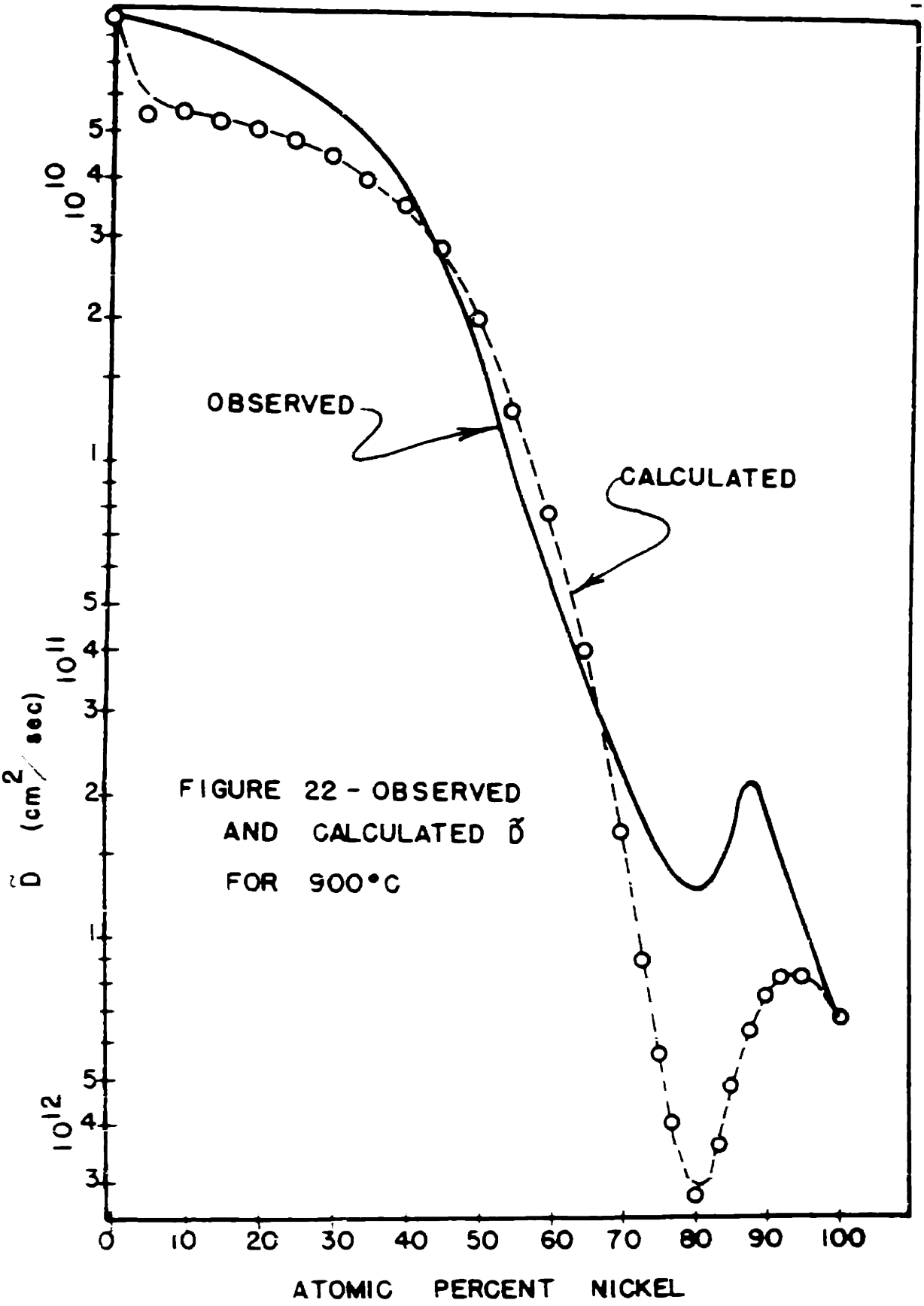

FIGURE 22 - OBSERVED AND CALCULATED $\tilde{D}$ FOR 900°C

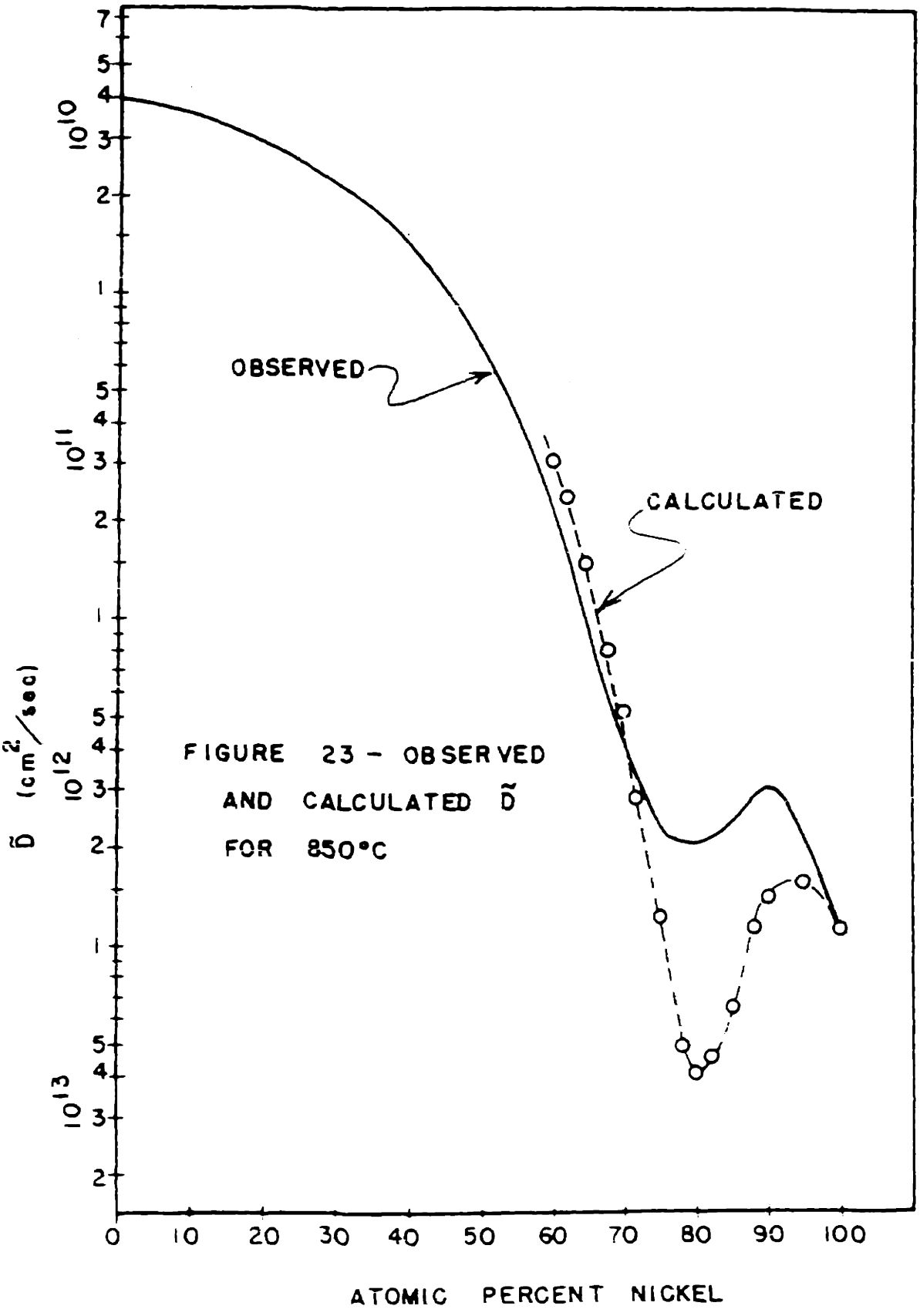

FIGURE 23 - OBSERVED AND CALCULATED $\tilde{D}$ FOR 850°C

contain plots of $\tilde{D}_{obs}$ and $\tilde{D}_{calc}$ as a function of concentration for 900 and 850°C respectively, and they appear in good agreement considering the multiplicity of experimental techniques involved. In view of the differences in the interdiffusion coefficients for pure metal couples at 900°C (see Figure 12), one may predict that the $\tilde{D}_{obs}$ values determined in the vicinity of the minimum by incremental couples would approach the $\tilde{D}_{calc}$ values if longer times were used for the diffusion anneals. The thermodynamic data at 850°C does not appear as consistent as that for 900°C and does not allow calculation over the entire range of concentrations. Furthermore the $\tilde{D}_{obs}$ values for 850°C in the vicinity of the minimum were definitely inconsistent with the remaining data (see Figure 15) and the extrapolated values were used. Appendix I contains a summary of the data and results for the calculation of $\tilde{D}_{calc}$ from D^*_{Au}, D^*_{Ni}, D_{Au}, D_{Ni}, and the thermodynamic data.

All experimentally determined diffusivities for the gold-nickel system for 900°C are plotted in Figure 24 as a function of atomic percent nickel. One of the dotted curves in this group is $(X_{Ni}\, D^*_{Au} + X_{Au}\, D^*_{Ni})$. It is clear from this that the actual $\tilde{D}$ for the non-ideal solution is influenced greatly by the thermodynamic factor, and the minimum is projected into the curve by the minimum in the thermodynamic factor.

Marker Movements and Porosity Calculations of marker velocities have been made by the use of equation (16) utilizing the available intrinsic diffusivities of gold and nickel and the slopes $(\frac{d\, X_{Ni}}{dy})$

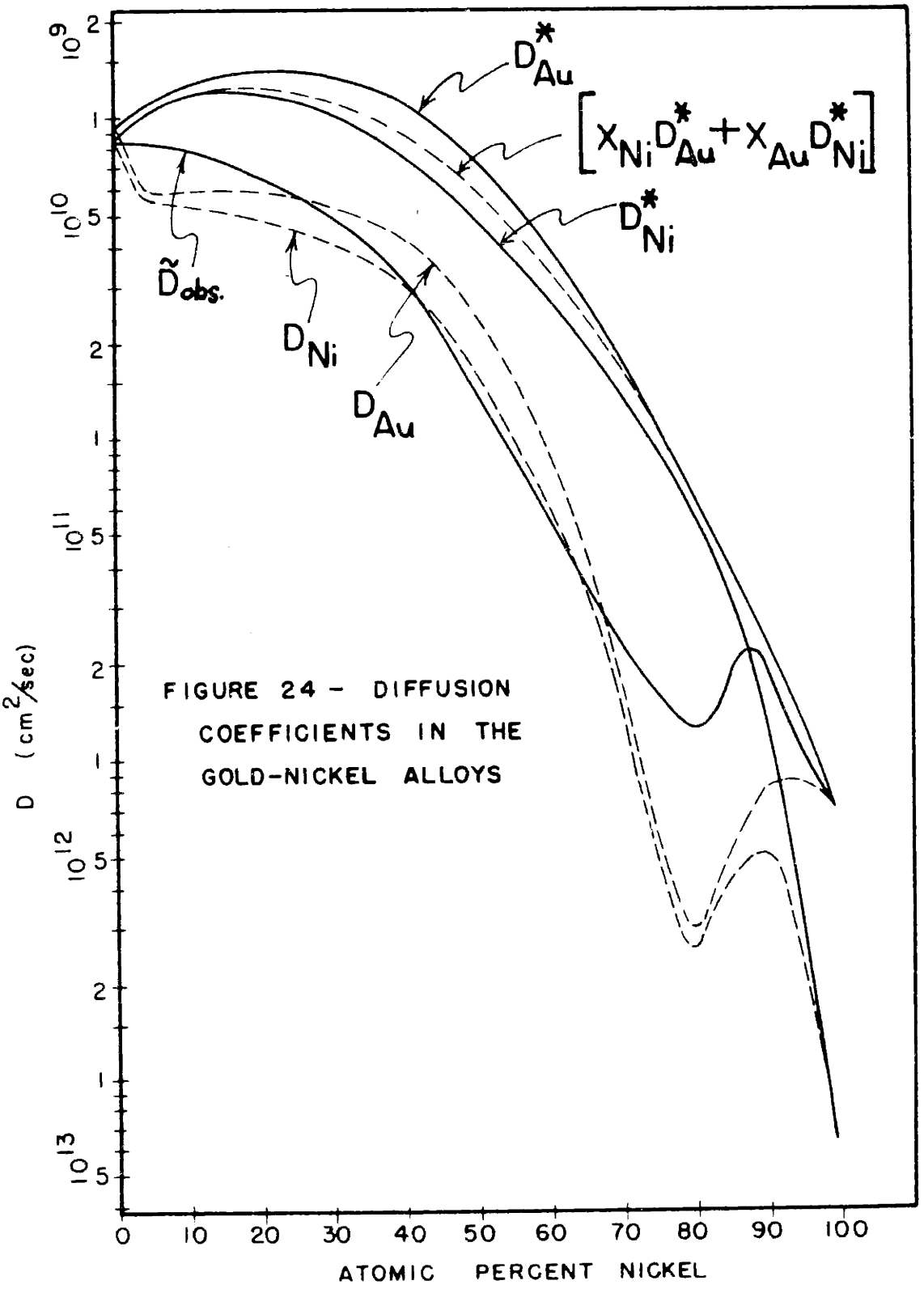

FIGURE 24 - DIFFUSION COEFFICIENTS IN THE GOLD-NICKEL ALLOYS

of the gradient curves. The slopes were taken at the experimental marker locations although such locations were in error. Since marker movements were small and the markers remained near the Matano interface, the error in slopes will be small. In effect, the slopes that are used here are practically the same as the slopes that would have been obtained had the markers been located accurately. Results of the calculations are given in Table XVI, and the magnitude of the marker movement for one of the runs is estimated as follows:

Run No. 2

Range: 0-100 atomic percent nickel, 900°C

$t = 25$ days $= 2.16 \times 10^6$ seconds

v_{calc} (see Table XVI) $= 0.61 \times 10^{-9}$ cm/sec

Δy = marker movement $= 2(v_{calc})(t) = 2(.0013)\,cm = .0026\,cm$

It is seen that the calculated marker movement is of the order of magnitude of the errors ($\pm$ .003 cm) involved in the attempts to measure them directly. Since $D_{Au} > D_{Ni}$ in all cases considered here, the markers should move toward gold-rich side of the couples.

Porosity The small amount of porosity found in some of the pure metal couples can be neglected here since these couples did not contribute to the final $\tilde{D}$ curves. It is also estimated that any errors in the interdiffusion coefficients due to such a small amount of porosity would be well within the experimental scatter. The porosity being found on the nickel-rich side of the couple contradicts the findings of Balluffi(12) and Seith and Kottmann(13). The reason

TABLE XVI

Data for the Calculation of Marker Velocities

Run No.	°C	$100X_{Ni}$	$\frac{dX_{Ni}}{dy}(cm^{-1})$	Atomic % Ni Range	$D^*_{Au}10^9$	$D^*_{Ni}10^9$	T.F.	$10^9 v_{calc}$ (cm/sec)
2	900	28	4.8	0–100	1.4	1.08	.40	.61
9	"	47.5	2.38	35–65	.84	.58	.36	.23
10	"	88.1	6.7	80–100	.053	.020	.23	.051
4	850	36.0	8.85	0–100	.58	.34	.32	.69
18	"	12.0	1.85	0–20	.61	.46	.41	.12
13	"	15.5	2.95	0–35	.64	.44	.39	.23
19	"	46.0	5.0	35–65	.42	.24	.28	.25
15	"	58.5	7.0	50–80	.19	.15	.21	.059
12	"	90.0	16.5	80–100	.0063	.0062	.23	.00039

$$v_{calc} = (D_{Ni}-D_{Au})\frac{\partial X_{Ni}}{\partial y} = (D^*_{Ni}-D^*_{Au})\left[1+\frac{\partial \ln f_{Ni}}{\partial \ln X_{Ni}}\right]\frac{\partial X_{Ni}}{\partial y}$$

$$T.F. = \left[1+\frac{\partial \ln f_{Ni}}{\partial \ln X_{Ni}}\right]$$

X_{Ni} is the approximate concentration at which marker was located.

for this discrepancy is not clear but a clue might lie in the morphology of the voids. Voids generated during diffusion are usually spheroidal or angular, but in the present case their shape was more like that of graphite flakes in grey cast iron.

V. CONCLUSIONS

1. Darken's phenomenological theory introducing intrinsic diffusivities and atomic mobilities with the chemical potential gradient as the driving force is valid for the gold-nickel system at temperatures between 850 and 900°C.

2. The magnitude of the errors due to molar volume changes in pure metal interdiffusion couples of the gold-nickel alloys are small and lie well within the experimental scatter of data.

3. For interdiffusion in the gold-nickel system, the pure metal couples do not give the same values of $\tilde{D}$ as those obtained from incremental couples. The reasons for this are uncertain, but may be due to the short circuiting paths resulting from the steep concentration gradient.

4. Marker velocities are so small that they cannot be measured accurately by the method used, but they agree in order of magnitude with the velocities calculated from the Darken equations.

5. Porosity is generated in the diffusion zone of pure metal couples of gold and nickel at temperatures between 875 and 925°C, but the quantity of porosity is relatively small. It is believed that this porosity is not due to a Kirkendall effect, but to the large stresses resulting from steep concentration gradients.

VI. SUGGESTIONS FOR FUTURE WORK

1. Additional interdiffusion runs with incremental couples of 65-100 atomic percent nickel would be expected to give closer agreement with the Darken equations if the diffusion anneal periods were three to six months.

2. It appears from the relative values of the intrinsic diffusion coefficients that the markers will move toward the gold-rich side of an interdiffusion couple. One might check the direction of movement by a single "foil-bend" test in a pure metal couple diffused for approximately one week.

3. An extensive study of marker movements might be instigated to determine marker velocities by a more sensitive method, for instance - using two sets of markers and measuring their distance apart for various time intervals. Results from this could be used to cross-check Darken's equations.

4. Work should be continued on porosity in gold-nickel couples since in the present work, porosity generated during interdiffusion was found on the nickel-rich side of the Matano interface while other investigators have found it to occur on the gold-rich side. The morphology of the voids was not conventional, and a study of this point may yield interesting results.

REFERENCES

1. C. Matano, Japanese Journal of Physics, 8 (1933) 109.
2. G. Grube and A. Jedele, Zs. f. Elektrochem., 38 (1932) 799.
3. A. Jedele, Ibid 39 (1933) 691.
4. L. S. Darken, Trans. A.I.M.E., 175 (1948) 184.
5. L. Onsager and R. M. Fuoss, J. Phy. Chem. 36 (1932) 2689.
6. U. Dehlinger, Z. Phys. 102 (1936) 633.
7. A. D. Le Clair, Progress in Metal Physics, Butterworths Scientific Publications (1949).
8. C. E. Birchenall and R. F. Mehl, Trans. A.I.M.E., 171 (1947) 143.
9. A. G. Guy, Trans. A.I.M.E., 185 (1949) 607.
10. L. L. Seigle, Thermodynamic Properties of Solid Nickel-Gold Alloys, Doctorate Thesis, M.I.T. (1952).
11. A. D. Kurtz, Diffusion in Gold-Nickel, Master's Thesis, M.I.T. (1952).
12. R. W. Balluffi, Personal Correspondence.
13. W. Seith and A. Kottmann, Angewandte Chemie, 64 (1952) 379.
14. A. D. Smigelskas and E. O. Kirkendall, Trans. A.I.M.E., 171 (1947) 130.
15. L. C. Correa de Silva and R. F. Mehl, Trans. A.I.M.E., 191 (1951) 155.
16. G. S. Hartley and J. Crank, Garaday Soc. Trans., 45 (1949) 801.
17. M. Cohen, C. Wagner, and J. E. Reynolds, J. of Metals, Nov.(1953) 1534.
18. E. C. Ellwood and K. Q. Bagley, J. Insti. of Metals, July(1952) 617.
19. W. A. Johnson, Trans. A.I.M.E., 143 (1941) 107.
20. A. M. Sagrubskij, Physikalische Zeitschrift der Sowetjunion, 12 (1937) 118.

21. H. C. Gatos and A. Azzam, Trans. A.I.M.E., 188 (1952) 407.

22. C. L. Raynor, L. Thomassen and L. J. Rouse, Trans. A.S.M. 30 (1942) 313.

23. J. Steigman, W. Shockley and F. C. Nix, Phys. Rev., 56 (1939) 13.

24. D. Turnbull, Phy. Rev., 76 (1949) 471A.

25. I. D. Bakalar, Doctorate Thesis M.I.T. (1951).

26. H. A. Jones, I. Langmuir and G. M. J. Mackay, Phys. Rev., 30 (1927) 201.

27. H. S. Carslaw and J. C. Yaeger, Conduction of Heat in Solids, (1947) 218, Oxford University Press, London.

28. L. Boltzmann, Weidem. Ann. Physik, 53 (1894) 959.

BIOGRAPHICAL NOTE

The author was born in Bessemer, Alabama, on January 21, 1923. He attended the public schools of that city; and he was graduated from the University of Alabama in August, 1944; with the degree of Bachelor of Science in Metallurgical Engineering. The following two years was spent in the USNR. After discharge from the armed services the author worked as Plant Metallurgist for Continental Gin and Company of Birmingham, Alabama, until 1947. At that time he entered the graduate school of the Missouri School of Mines where he received the degree of Master of Science in Metallurgical Engineering in June, 1948. The following year was spent as Instructor of Metallurgical Engineering at the Missouri School of Mines. In the fall of 1949, he entered M.I.T. as a candidate for the degree of Doctor of Science.

APPENDIX A

Corrections for Molar Volume Changes

It has been shown (16,17) that if there is a molar volume change in the diffusion zone of a Matano couple, the normal form of Fick's first law, equation (A-1), is not rigorous since the measurement of distances (y) becomes ambiguous.

$$J_i = -D \frac{\partial c_i}{\partial y} \qquad (A-1)$$

where the flux, J_i, is the quantity of the i-th component which diffuses per unit time through unit area of a plane at right angles to the direction of diffusion. The concentration c_i is defined by

$$c_i = \frac{X_i}{V} \qquad (A-2)$$

If the molar volume (V) is constant, using equations (A-1) and (A-2) one obtains

$$J_i = -\frac{D}{V} \frac{\partial X_i}{\partial y} \qquad (A-3)$$

When molar volume is not constant modifications deviating from the orthodox linear scale in centimeters for measuring distance in the diffusion direction may be made to compensate for volume changes on mixing, and methods of correcting for molar volume change in the diffusion zone have been described by Cohen, Wagner, and Reynolds(17). One method entails the use of the distance parameter

defined by equations (A-4) and (A-6)

$$d\xi = \frac{dy}{a^3} = \frac{dy}{V_a} \tag{A-4}$$

where a is the local lattice parameter and V_a is the cell volume. The cell volume in terms of molar volume is

$$V_a = \frac{\text{molar volume}}{\text{unit cells per mole}} = \frac{V}{N_o/4} = \frac{4V}{N_o} \tag{A-5}$$

and substituting equation (A-5) in equation (A-4), one obtains

$$d\xi = \frac{N_o}{4} \frac{dy}{V}$$

or

$$dy = \frac{4V}{N_o} d\xi \tag{A-6}$$

The units of ξ are $\frac{\text{atoms}}{\text{moles}}$. Considering equations (A-3) and (A-6), and temporarily assuming V constant to find the relation between $\tilde{D}$ and $\tilde{D}_\xi$, Fick's first law takes the form

$$J_i = -\frac{N_o \tilde{D}}{4 V^2} \frac{\partial X_i}{\partial \xi} \tag{A-7}$$

or

$$J_i = -\tilde{D}_\xi \frac{\partial X_i}{\partial \xi} \tag{A-8}$$

and $\tilde{D}_\xi$ is the interdiffusion coefficient corresponding to the measure of concentration as mole fraction, and distance by the parameter ξ as defined above. The parameter ξ can be evaluated by graphical integration of equation (A-4) if the lattice parameter is known as a function of concentration. The interdiffusion coefficient $\tilde{D}_\xi$ is obtained by the Boltzmann-Matano treatment of an X-ξ curve, and the relation between the modified and the conventional inter-

diffusion coefficients is

$$\tilde{D} = \tilde{D}_{\zeta} \cdot \frac{4V^2}{N_o}$$

$$(cm^2/sec) = \left(\frac{\text{unit cell}^2}{\text{sec cm}^4}\right) \frac{cm^6}{(\text{unit cell})^2} \qquad (A-7)$$

The large difference in atom size between gold and nickel leads one to expect an appreciable error in $\tilde{D}$ when the conventional distance parameter (y) is used. In this system the molar volume is approximately a linear function of mole fraction, and there will thus be a negligible change in the overall volume. However, the local molar volume changes are appreciable and will introduce errors in the measurements of distance when y is used since distance is measured from the Matano interface into the zone of diffusion.

Molar volume change corrections using ζ were applied to the X-y data from a gold-nickel couple, and the results are given in Table A-I and plotted in Figure A-1 along with the experimental values calculated without volume corrections. This plot shows the magnitude of this correction to be unimportant. For comparison purposes the results of a c-y calculation have also been entered, where c has been taken as X_{Ni}/V. The curves for (X-y) and (c-y) appear to be identical within experimental scatter, but these curves differ from the (X-ζ) curve except in the intermediate concentrations.

TABLE A-I

Experimental $\tilde{D}$ Values

For Different Methods of Calculation

Atomic Percent Nickel	$10^{10}\ \tilde{D}$ cm²/sec		
	Plot: x-y	Plot: x-ζ	Plot: c-y
5	6.16	6.85	6.67
10	6.26	6.41	6.08
25	2.57	5.84	5.77
40	2.97	2.80	2.74
50	1.80	1.83	1.67
55	1.50	-	-
60	1.24	.98	1.13
65	1.13	-	-
70	.86	-	-
72	.78	-	-
74	.74	-	-
75	-	.71	.78
78	.83	-	-
80	.82	.73	-
84	.86	-	-
88	.83	-	-
90	.81	.73	-
91	-	-	.80

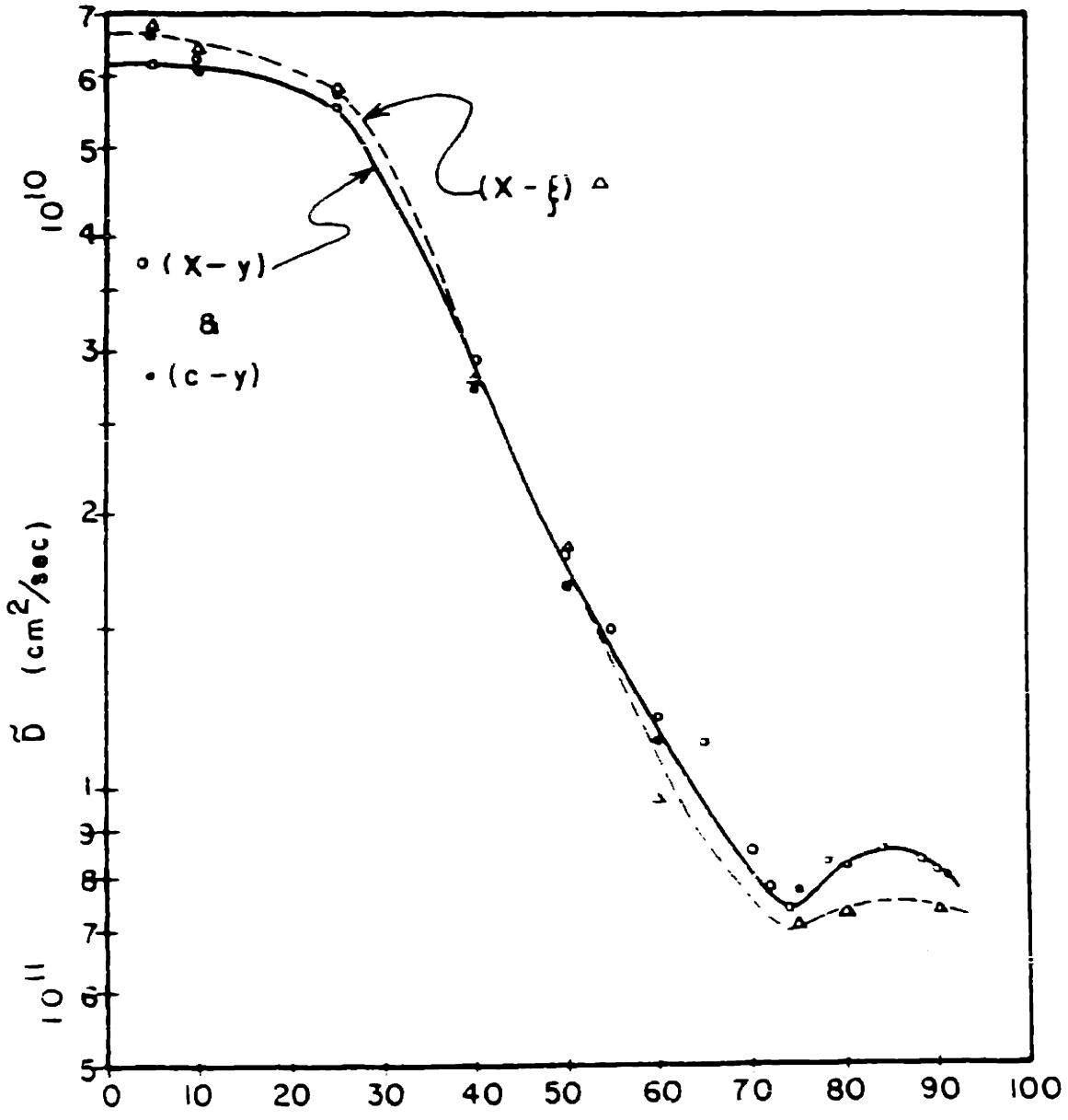

FIGURE A-1 - EXPERIMENTAL $\tilde{D}$ FOR DIFFERENT METHODS OF CALCULATION

APPENDIX B

Procedure for the Recovery Of Metallic Ni^{63} from Chloride Solution

A total volume of 19.4 ml of nickel chloride in an HCl solution of 0.38 normality was received from Oak Ridge. The procedure for the electrolytic recovery of the isotope in metallic form is given below.

An equal volume of concentrated H_2SO_4 was added to the 19.4 ml of the isotope solution. The excess HCl was boiled off and boiling was continued until dense white fumes of SO_3 began coming off. A white precipitate formed, presumably nickel sulfate, but this dissolved upon diluting with distilled water to 30 ml and reheating. The resulting solution was then brought to an approximate pH of 7 by adding NH_4OH dropwise. This solution was used as an electrolyte in a cell utilizing a stainless steel anode spaced approximately 3/8" from a molybdenum cathode. The electrodes were flat and the area of each was approximately 12 square centimeters. Metallic Ni^{63} was deposited on the cathode with the cell operating at 1.5 amps and 5 volts for 2 hours. The cathode was removed, rinsed in distilled water, acetone, and benzene respectively. Using the foregoing procedure, the deposit of metallic nickel did not adhere to the molybdenum cathode and was easily flaked off. Estimated recovery of the nickel from the electrolyte was approximately 80%.

APPENDIX C

Melting Technique for Preparation of Alloys

A schematic drawing of the melting apparatus is shown in Figure C-1. Induction melting was used exclusively with a quartz tube as a crucible. Loose fitting cylinders of the desired weights (usually 100 to 150 grams total) of nickel and gold were placed in the quartz tube, and the tube was evacuated using a mechanical pump and flushed several times with argon. With the vacuum full on, it was found that the melt boiled vigorously when the gold content was high. There was greater danger of the quartz tube collapsing during melting under vacuum, although better heating resulted due to the additional insulation. Optimum argon pressure during melting was, therefore, somewhat variable, but generally $\frac{1}{4}$ to $\frac{1}{2}$ atmosphere of argon was used during the later melting stages of the high gold alloys with tendencies toward higher vacuum at higher nickel.

After melting was completed, a soaking period of 5 to 10 minutes was allowed. The quartz tube was then removed from the furnace coils and the bottom end placed gently in water for rapid freezing with controlled directional solidification. Up to one-third of some ingots were lost due to pipes, but almost one hundred percent ingot yield was obtained when an asbestos hot top was used during solidification. The asbestos hot top was made by wrapping strip

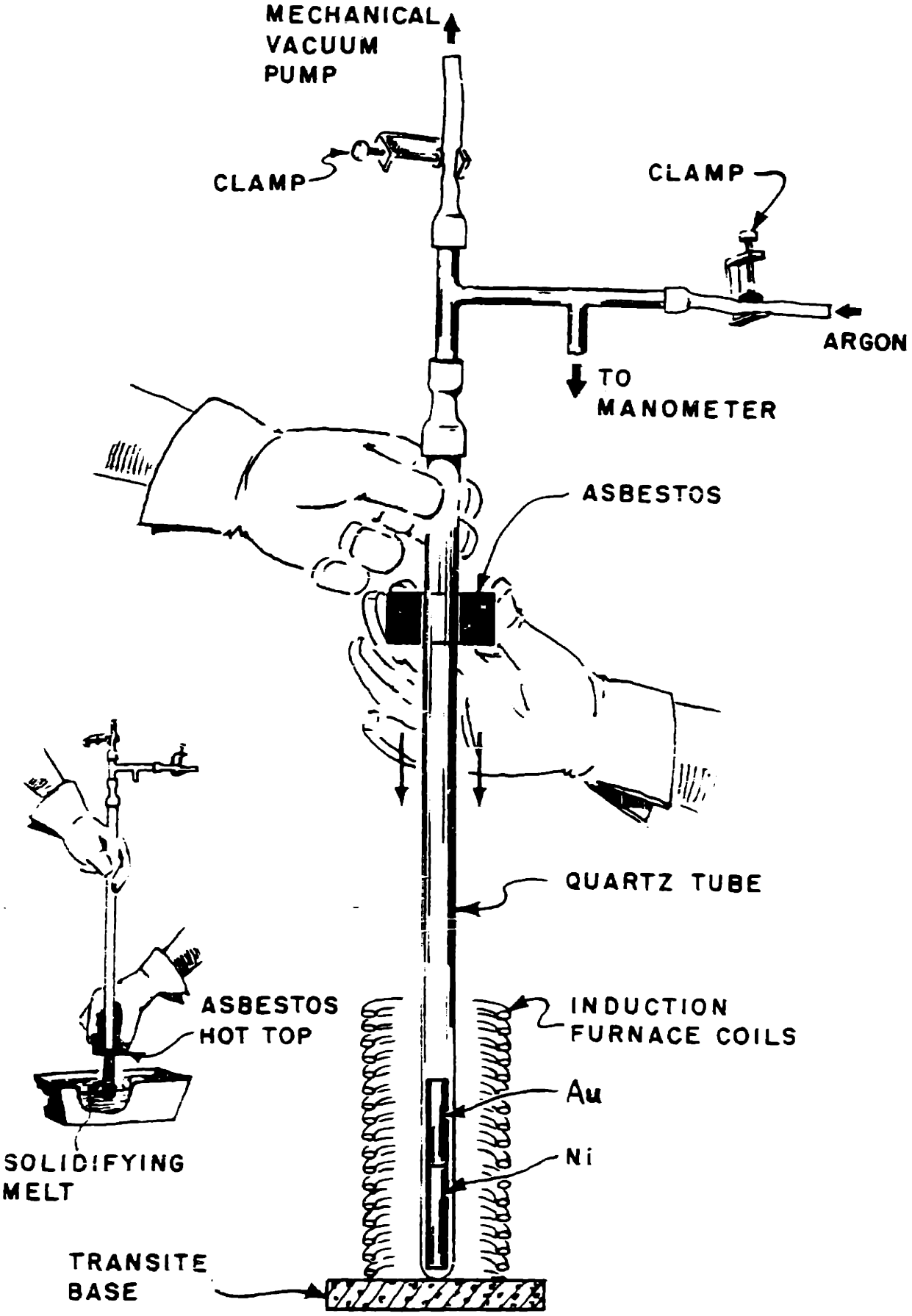

FIGURE C-1 - SETUP FOR MELTING Au-Ni ALLOYS

asbestos around the quartz tube, and it was held near the top of the tube during melting, sliding it into place when solidification began. The sealed end of the quartz tube had to be broken after each melt to remove the ingot but could be resealed and the tube reused until it became too short to handle with comfort and safety.

Occasional segregation up to two atomic percent over a four-inch length was found, but this was believed due to insufficient soaking periods and such segregation was eliminated by remelting. Chemical analysis of approximately three-fourths of the ingots was made of samples taken at intervals of $\frac{1}{4}$ inch over the entire length, and the average variation of composition was 0.1 atomic percent per inch.

A melt of pure nickel was checked for silicon pickup to see if a harmful amount of silicon would be picked up from the quartz melting tube. It was ascertained by chemical analysis that the silicon in the nickel increased from 0.0045 weight percent to 0.013 weight percent, which was believed not excessive.

APPENDIX D

Evaporation Unit

Evaporation of thin films of Ni^{63} onto gold-nickel specimens was accomplished by placing the Ni^{63} on a tantalum filament and heating it to approximately 1600°C in a high vacuum (10^{-5} mm Hg) chamber. Such a unit was built under the supervision of Kurtz and Gatos and was modeled after an evaporator in the M.I.T. corrosion laboratory. The details of the unit are shown in Figure D-1. A complete description has been given by Kurtz(11) and will not be repeated here. A few points will be mentioned, however, which are perhaps unique in the use of this equipment in work with nickel.

Evaporation of Ni^{63} is best accomplished at temperatures not far above the melting point. If the temperatures get too high then the deposited layer darkens, and this has been attributed to oxide formation which may lead to inferior bonding during the subsequent welding operation. The efficiency (approximately 30 percent maximum) is controlled by the radiating angle (which can be varied somewhat by adjusting the sides of the well in the tantalum boat) and the distance separating the Ni^{63} charge from the specimen surface (which should be a minimum of 3/8 inch for a ½-inch diameter specimen or a nonuniform layer of the isotope will result). The uniformity of the layer was tested by exposure to no-screen X-Ray film, and several specimens were discarded upon the basis of this test. Care must also be taken to prevent any abrasion of the surface after the deposition or a loss of boundary conditions may result.

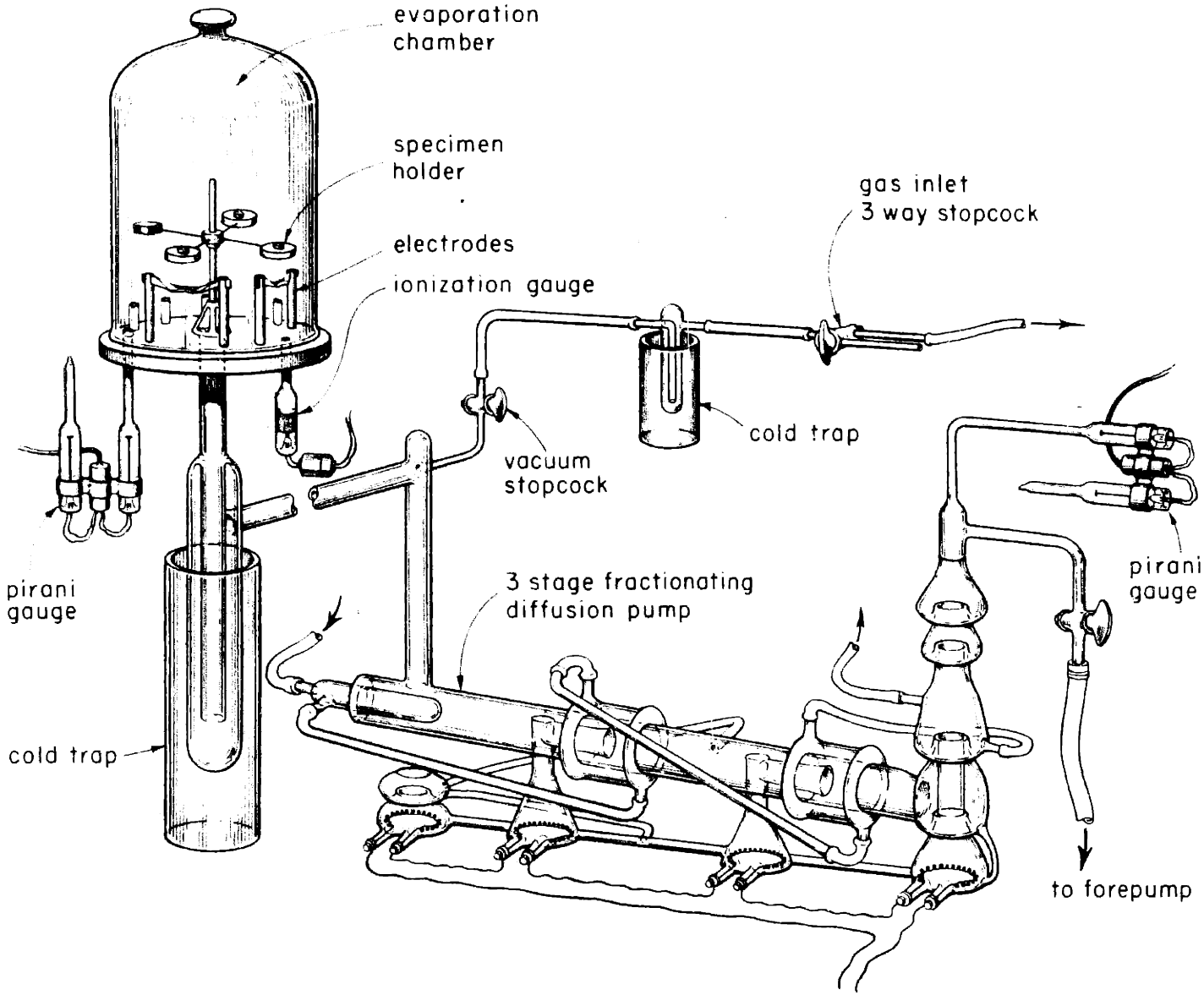

FIGURE D-1 – DETAIL OF VACUUM SYSTEM

APPENDIX E

Preparation of Specimens For Counting Using Ni^{63} Tracer

After the diffusion anneal and the specimens were sectioned, no activity was detected with the conventional end-window counter because of the high absorption by the air and the counter window. Thus, the use of a windowless flow counter was essential in the present work. In this type of counter the registration of the β particles is practically 100 percent efficient and counting rates up to 5000 counts per minute were obtained for each slice.

When relative counting rates are desired the problem of obtaining a constant geometry from sample to sample is acute. This is particularly so with Ni^{63} because of the low energy β. A flow sheet of the procedure for obtaining suitable geometry is shown in Figure E-1.

Four points which favor good counting geometry are: (1) lower absorption, (2) more active tracer element, (3) higher concentration of tracer element, and (4) smaller sample size. Since factors one and two were limited in the present case the geometry was improved by using a concentration of the tracer element sufficiently high and simultaneously decreasing the size of the sample counted.

Since a flow counter was used, great care was necessary to prevent contamination of the Geiger chamber with moisture, hence the use of the drying oven and transferral of the specimens directly from the oven to the counter preflush chamber. This is particularly serious due to the hygroscopic nature of nickel chloride. For instance, oven dried samples gave a counting rate 50 percent lower after sitting overnight in a dessicator.

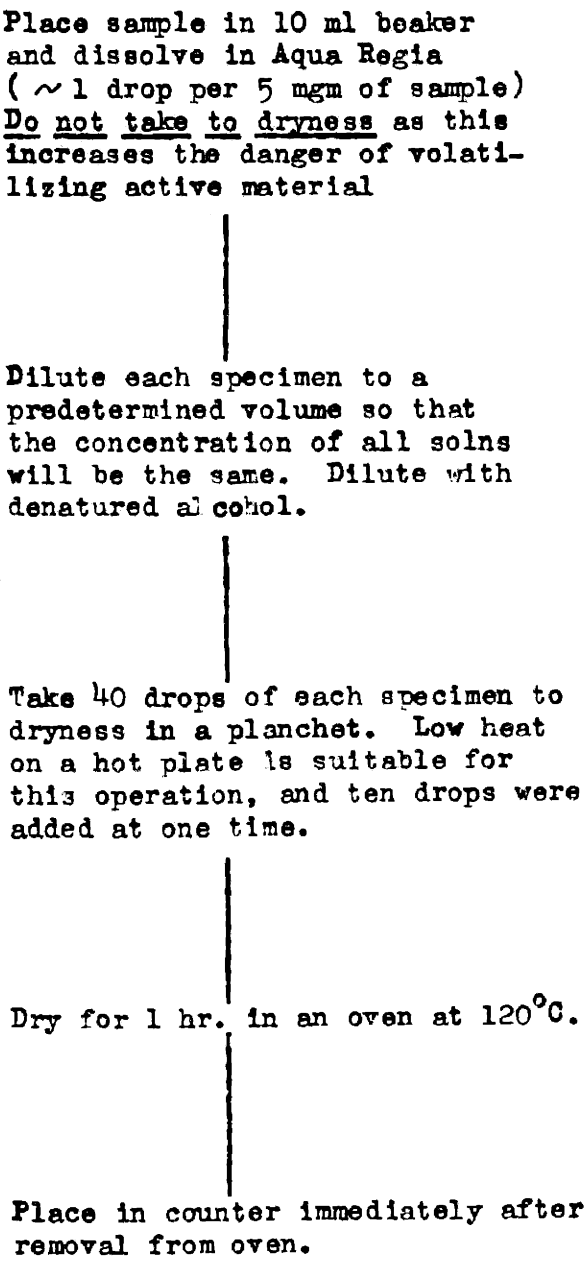

Figure E-1-Flow Sheet for Preparation of Au-Ni Specimens for Counting

APPENDIX F

Typical Calculation Of D^*_{Ni} Using the Sectioning Technique

With an instantaneous plane source of the radioactive material diffusing into both sides of the couple the mathematics are analogous to that given by Carslaw and Jaeger(27) for heat flow, and previously stated in equations (20), (21), and (22). Equation (22) is the most useful form here.

$$\frac{d \log c}{d y^2} = \frac{-1}{9.20 D^*_{Ni} t} \qquad (22)$$

where D^*_{Ni} is the radioactive diffusion coefficient in cm^2/sec, c is the concentration (which is proportional to the counting rate) of the isotope at y distance from the original join, t is the time of diffusion in seconds, and c_o is the concentration of isotope at the interface at t = 0. Plotting c on a log scale against y^2 on a linear scale will allow calculations of the diffusion coefficient from the slope when time is known.

An example of this calculation is contained in Table F-1 and Figures F-1 and F-2. The y values in Table F-1 represent the midpoints of the slices.

Data are smoothed in Figure F-1 by plotting counts per minute above background versus y, and the interface (y = 0) is located from the symmetry of the curve. After measuring y from the interface and

TABLE F-I

Data for the Determination

Of D^{*}_{Ni} in Pure Gold by the Sectioning Method

Slice No.	Wt. of Slice (mgm)	$10^3\Delta y$(cm)	$10^3 y$(cm)	Counts per min. Above background
1	97.4	5.260	2.63	41
2	107.9	5.827	8.17	95
3	81.5	4.401	13.3	207
4	90.3	4.876	17.9	347
5	102.5	5.535	23.1	705
6	101.2	5.465	28.6	1289
7	91.1	4.919	33.8	1924
8	111.8	6.037	39.3	3118
9	97.5	5.265	44.9	4355
10	81.0	4.374	49.8	5508
11	96.6	5.216	54.6	4206
12	84.4	4.558	59.4	4455
13	69.0	3.726	63.6	3957
14	85.0	4.590	67.8	3794
15	112.8	6.091	73.1	2808
16	82.6	4.460	78.4	1600
17	100.0	5.400	83.3	1149
18	96.5	5.211	88.6	605
19	81.2	4.385	94.4	538
20	97.7	5.276	98.2	155
21	105.2	5.681	103.7	69
22	92.9	5.017	109.1	30

ρ = density of alloy

d = diameter of couple = 0.4345 inches

T = 904°C

t = 1.58×10^5 sec

Δy = thickness of slice in centimeters (10^3) = $\frac{\text{wt. in mgm}}{5.06\, d^2 \rho}$

= .0540 x (weight in milligrams)

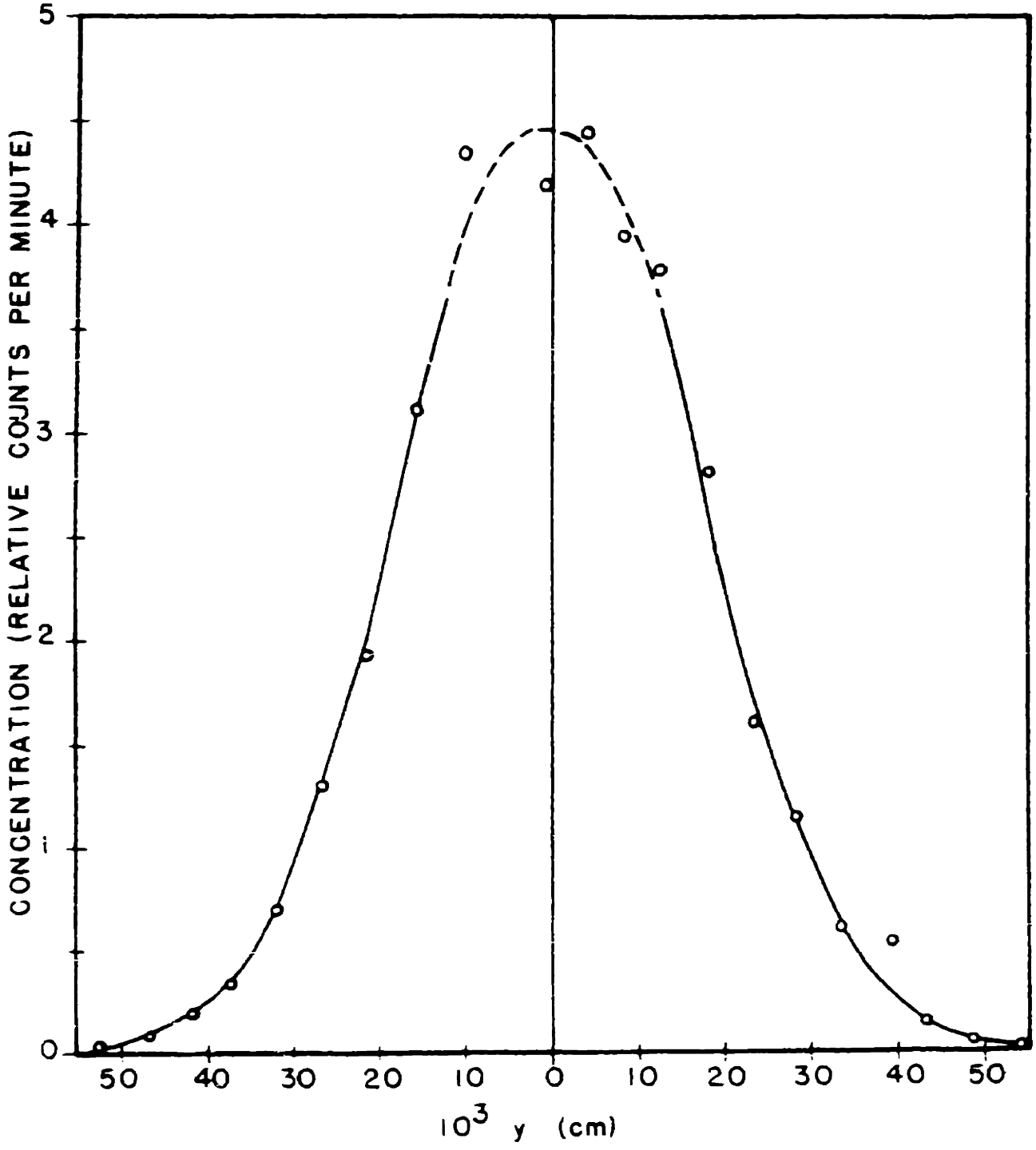

FIGURE F-1 - CONCENTRATION (RELATIVE COUNTS PER MINUTE) — DISTANCE CURVE FOR THE DIFFUSION OF Ni^{63} IN PURE GOLD AT 904°C

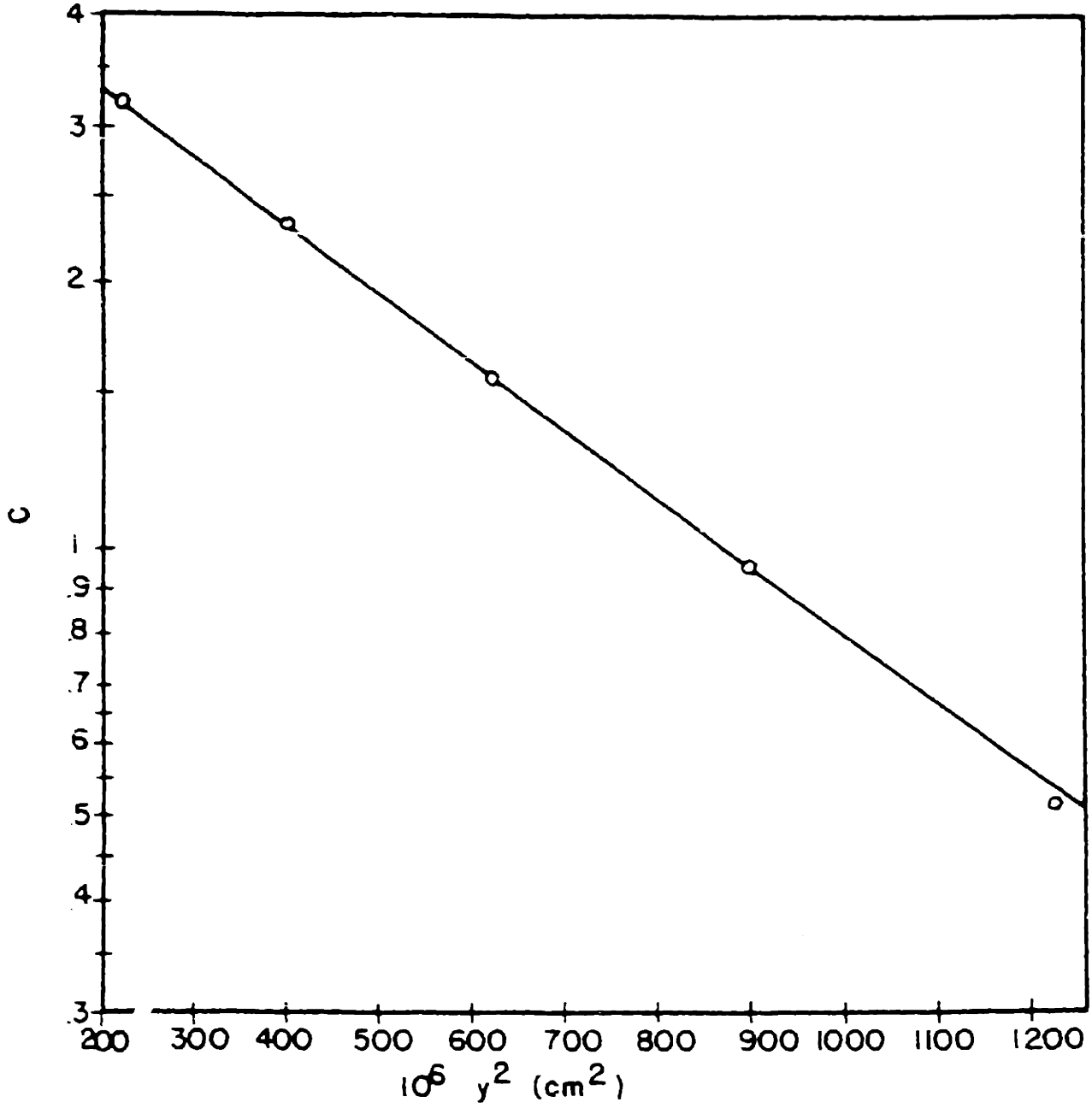

FIGURE F-2 – CONCENTRATION – $\overline{\text{DISTANCE}}^2$ FOR THE DIFFUSION OF Ni^{63} IN PURE GOLD

obtaining the corresponding values of c, the plot log c versus y^2 was made in Figure F-2. From Figure F-2:

$$\text{Slope} = \frac{\log 3/.3}{10^{-6}(258-1560)} = \frac{-.1086}{D^*_{Ni} \times 1.58 \times 10^5}$$

$$D^*_{Ni} = 8.96 \times 10^{-10} \text{ cm}^2/\text{sec}$$

Errors

Counting Because of the statistical nature of radioactive disintegrations a sufficiently large number of counts are necessary in order to minimize the errors in counting. Counting errors as a function of the ratio of total number of counts to background counts are given in Figure F-3. In the present work this ratio was usually kept sufficiently large so that the error due to counting was less than 1 percent.

Counting Geometry This error is the largest source of error in the experiment due to the high absorption of the low energy β particle making it difficult to get reproducible geometry from specimen to specimen. Scatter in some instances probably gave as much as 20 percent error in D^*_{Ni} due to shape of curve and difficulty in locating the interface. It is believed that this error was generally less than 10 percent.

Temperature Considering the temperature dependency and magnitude of the diffusivities, a variation of $1^\circ C$ for a diffusion temperature of $900^\circ C$ will give an error in D^*_{Ni} of 1.5 to 2 percent depending on the concentration. Temperature control was $\pm 2^\circ C$ in the present work, and this error is estimated to be 3 to 4 percent maximum.

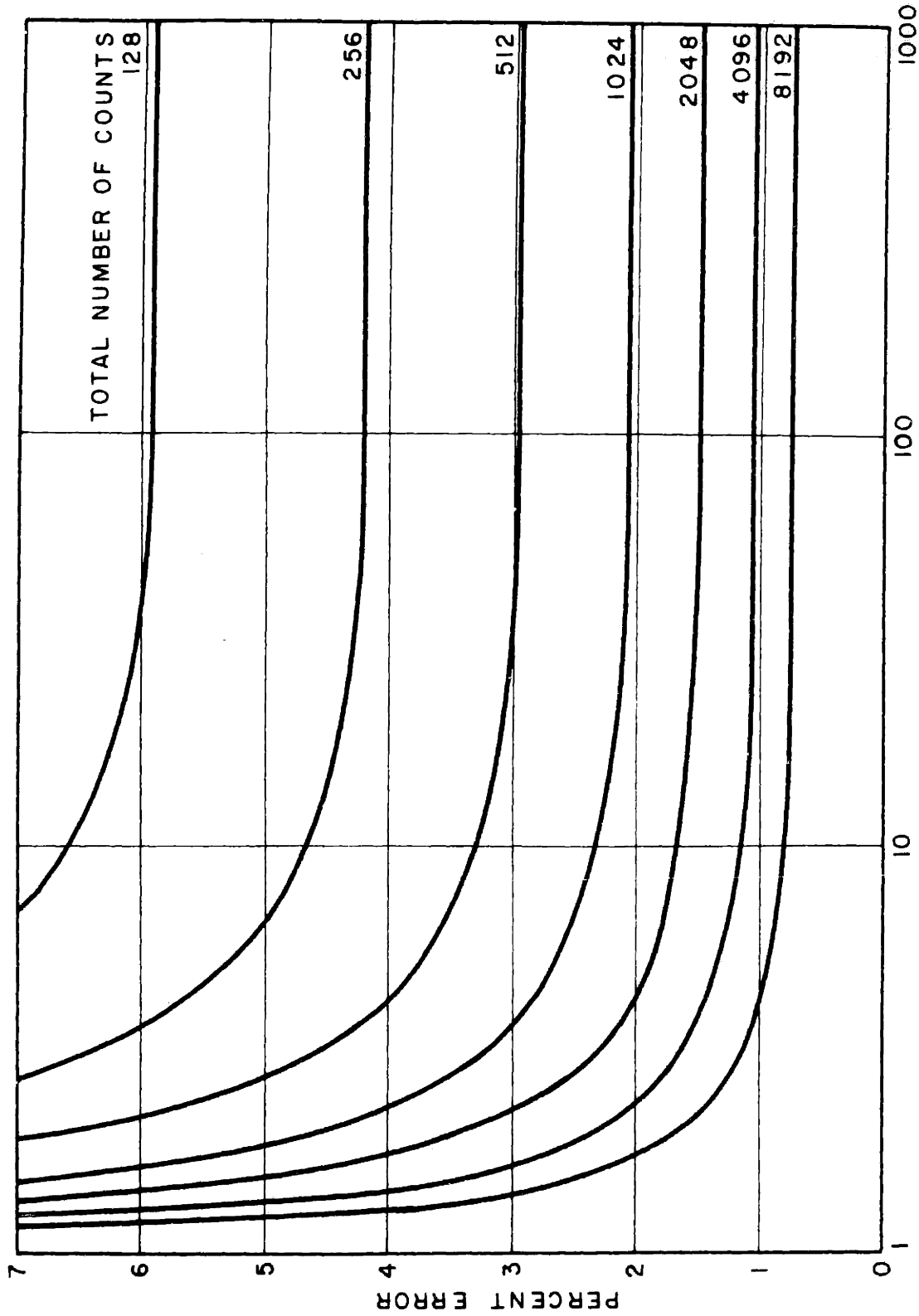

FIGURE F-3 - STATISTICAL COUNTING ERRORS

Time Length of time at the diffusion anneal temperature was sufficiently long to give negligible errors in the measurement of time. The time to reach the diffusion temperature was also small in comparison to the total time of diffusion. Errors due to the welding of the couple were negligible assuming no serious effects of stress.

Sectioning It is believed that the error due to the thickness of slice measurement may be neglected since each slice was weighed and its thickness calculated from the diameter and density. The error due to misalignment in the lathe is estimated to be less than 3 percent.

Summary of Errors

	Percent
Counting	1
Counting geometry	10
Temperature	4
Misalignment	3
Total Error	18

It should be pointed out that the above treatment gives the maximum probably error, and in many runs the individual errors may have been compensating thus giving an overall error less than 18 percent.

APPENDIX G

Calculation of Interdiffusion Coefficients

Boltzmann(28) and Matano(1) have shown that when Fick's second law is valid and the couple is semi-infinite, then concentration is a single-valued function of the auxiliary variable

$$\lambda = y/\sqrt{t} \qquad (G\text{-}1)$$

provided that the plane $y = 0$ is chosen so that

$$\int_{C_1}^{C_2} y\,dc = 0 \qquad (G\text{-}2)$$

Substituting equation (G-1) in equation (12) and integrating between the proper limits, equation (G-3) is obtained.

$$\tilde{D}(c) = -\frac{1}{2dc/d\lambda} \int_{C_1}^{C} \lambda\,dc$$

$$= -\frac{1}{2t}\,\frac{dy}{dc} \int_{C_1}^{C} y\,dc \qquad (G\text{-}3)$$

Using equation (G-3) in conjunction with a c-y curve, $\tilde{D}(c)$ may now be calculated graphically, taking c as equal to the atomic percent nickel.

Data for Run 7 is given as a numerical example of this calculation. The c-y curve obtained from sectioning and chemical analysis after the diffusion anneal is given in Figure G-1. The Matano interface ($y = 0$) is located according to equation (G-2) by equalizing the areas under the curve on either side of the interface. Reciprocal slopes

(dy/dc), and areas $(\int_{c_1}^{c} y\,dc)$ are taken for each value of c for which interdiffusivities are desired. Knowing the time of diffusion, equation (G-3) yields $\tilde{D}(c)$ values which are contained in Table G-I.

Errors

Temperature This error is similar to that already treated for D^{*}_{Ni} and is estimated to be 3 to 4 percent maximum.

Time Since the time of diffusion was greater than 13 days, no error was introduced due to time at welding temperature or in the heating or cooling.

Sectioning The thickness of the layers taken for analysis was measured to an accuracy of $\pm$ 0.0005 inch, and it is estimated that with smoothing of data this error is kept below 1 percent. The misalignment error was believed to be less than 4 percent.

Accuracy of Chemical Analysis This factor depended somewhat upon the concentration but was usually less than 1 percent.

Location of Interface Small errors in the location of the Matano interface do not affect the value of $\tilde{D}$ appreciably unless the curves are very steep. This error is of the order of 2 percent.

Tangent Measurement Since all tangents used were the results of at least six measurements by at least two persons this error is estimated to be less than 5 percent in all cases. Values of $\tilde{D}$ were not calculated too near the concentration limits where this error becomes prohibitive.

Area Measurements Areas under the c-y curves were measured with a planimeter, the error being less than 3 percent if readings are kept within the intermediate concentration ranges.

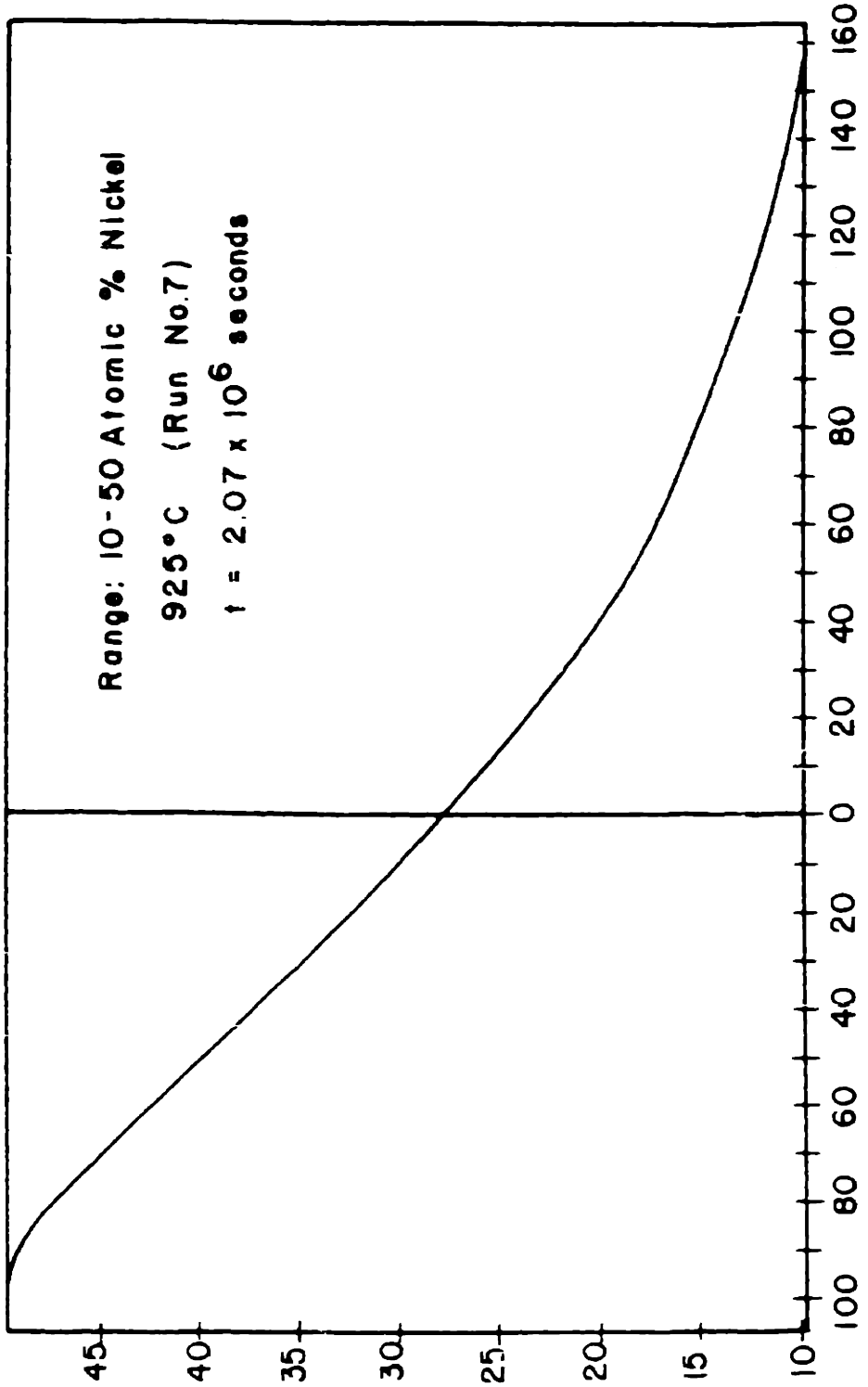

FIGURE G-1 - TYPICAL CONCENTRATION-PENETRATION CURVE FOR MATANO ANALYSIS

TABLE G-I

Data for Boltzmann-Matano

Calculation of Interdiffusion Run 7

Atomic Percent Nickel	$10^3 \frac{dY}{dc}$	$\int_{c_1}^{c} Y dc$ area	$10^9 \tilde{D}$ cm²/sec
15	10.1	.600	1.46
20	5.9	.883	1.26
25	4.7	.996	1.13
30	4.23	1.01	1.04
35	3.95	.888	0.848
40	3.93	.700	0.670
45	3.93	.38	0.36

$t = 2.07 \times 10^6$ sec

$T = 925^\circ C$

APPENDIX H

Sensitivity of Porosity Detection

Several layers of annealed fine gold wire (0.005-inch diameter) were wound on a bakelite spool and the entire unit mounted so that a tranverse section of the layers of wire was obtained. Polishing was carried out by hand lapping through 3/0 emery paper followed by canvas, broadcloth, and velveteen wheels using levigated alumina in a water suspension. A photomicrograph of the resulting structure is given in Figure H-1.

An estimation of the sensitivity of porosity detection was made by examining the area of contact between the wires in Figure H-1 as follows:

0.25 mm = minimum clean cut separation of wires

525 = linear magnification

$$\frac{0.25}{525} = 0.48 \times 10^{-3} \text{ mm or } 0.5 \text{ micron} = \text{porosity detection sensitivity}$$

Resolving power of the microscope using an objective lens of 0.65 N.A. and conventional illumination is not a limiting factor here. The approximate minimum dimension of a void that can be detected by the above technique is 0.5 micron.

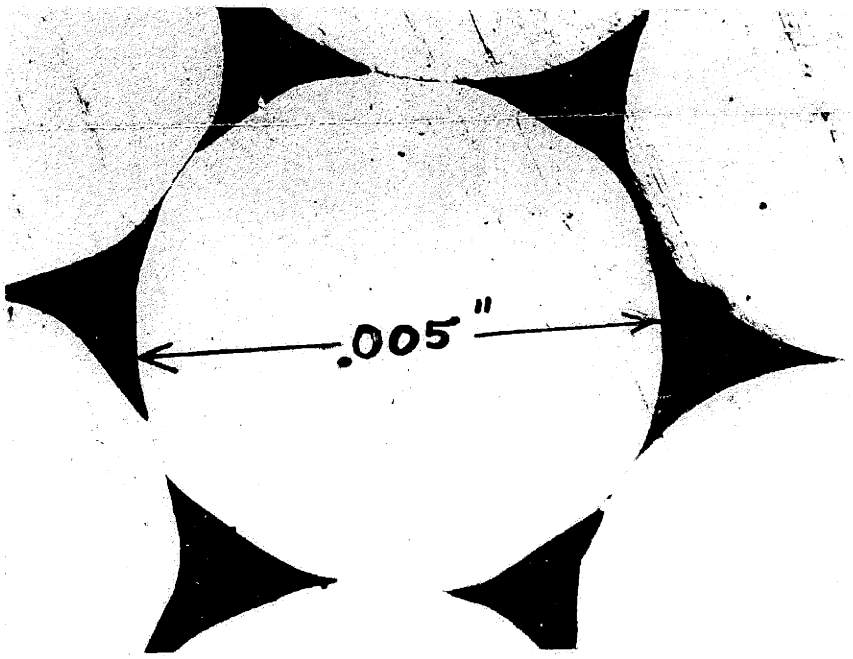

Figure H-1 525X

Cross Section of Gold Wire for Determining Porosity Detection Sensitivity

APPENDIX I

TABLE I-I

Summary of Data for Calculation of Interdiffusion Coefficients ($\tilde{D}_{calc}$) at 900°C

X_{Ni}	$10^9 D^*_{Ni}$	X_{Au}	$10^9 D^*_{Au}$	T.F.+	$10^9 D_{Ni}$	$10^9 D_{Au}$	$10^9 \tilde{D}_{calc}$
0	.87	1.00	.92	1.00	.87	.97	.87
.05	1.00	.95	1.12	.531	.531	.595	.543
.10	1.15	.90	1.28	.47	.541	.601	.550
.15	1.17	.85	1.38	.435	.509	.601	.522
.20	1.15	.80	1.4	.420	.483	.587	.504
.25	1.10	.75	1.4	.407	.448	.569	.48
.30	1.03	.70	1.34	.40	.412	.536	.448
.35	.91	.65	1.23	.40	.364	.492	.408
.40	.76	.60	1.1	.397	.302	.437	.356
.45	.61	.55	.92	.378	.231	.348	.284
.50	.47	.50	.75	.335	.157	.251	.204
.55	.36	.45	.57	.275	.0990	.157	.131
.60	.275	.40	.41	.220	.0605	.0902	.0784
.65	.205	.35	.28	.160	.0328	.0448	.0406
.70	.145	.30	.175	.100	.0145	.0175	.0167
.73	.115	.27	.13	.070	.00805	.0091	.00882
.75	.097	.25	.11	.053	.00513	.00583	.0056
.77	.082	.23	.09	.045	.00369	.00405	.00396
.80	.060	.20	.068	.042	.00252	.00285	.00278
.82	.050	.18	.055	.060	.00300	.0033	.00325
.85	.034	.15	.0405	.120	.00408	.00486	.00474
.88	.0215	.12	.029	.225	.00484	.00653	.00632
.90	.015	.10	.023	.335	.00503	.00771	.00744
.92	.0105	.08	.0185	.455	.00478	.00843	.0081
.95	.0045	.05	.0130	.645	.0029	.00839	.00814
1.00	.00062	0	.0068	1.00	.00062	.0068	.0068

+ $T.F. = \left[1 + \frac{\partial \ln f_{Ni}}{\partial \ln X_{Ni}}\right]$

All D-values given in $cm^2/sec.$

TABLE L-II

Summary of Data for Calculation

Of Interdiffusion Coefficients ($\tilde{D}_{calc}$) at 850°C

X_{Ni}	$10^{10} D^{*}_{Ni}$	X_{Au}	$10^{10} D^{*}_{Au}$	T.F.+	$10^{10} \tilde{D}_{calc}$
.60	1.36	.4	1.65	.2	.307
.62	1.23	.38	1.4	.18	.240
.65	1.06	.35	1.05	.142	.150
.68	.86	.32	.750	.103	.0809
.70	.75	.30	.60	.08	.0516
.72	.65	.28	.50	.052	.0282
.75	.48	.25	.35	.032	.0122
.78	.36	.22	.25	.018	.00493
.80	.28	.20	.2	.019	.00410
.82	.23	.18	.156	.027	.00457
.85	.14	.15	.115	.055	.00655
.88	.085	.12	.080	.140	.0113
.90	.061	.10	.063	.225	.0142
.95	.017	.05	.034	.505	.0155
1.00	.002	0	.011	1.000	.0110

+ $T.F. = \left[1 + \frac{\partial \ln f_{N_i}}{\partial \ln X_{N_i}}\right]$

All $\tilde{D}$-values given in cm^2/sec.